

TECHNICAL UNIVERSITY OF CRETE

School of Electronic and Computer Engineering



COHERENT DETECTION AND CHANNEL CODING FOR  
BACKSCATTER SENSOR NETWORKS

by

Nikos Fasarakis-Hilliard

Submitted in August, 2014 in partial fulfilment of the  
requirements for the Electronic and Computer Engineering  
Master of Science degree.

THESIS COMMITTEE

Associate Professor Aggelos Bletsas, *Thesis Supervisor*

Associate Professor George N. Karystinos

Associate Professor Antonios Deligiannakis

This Page Intentionally Left Blank

## Abstract

*With rapid advances in sensor technology and the evolution of scatter radio systems, the principle of reflection rather than active transmission employed by backscatter sensor networks has emerged as a potential key element of low-cost, large-scale, high-resolution ubiquitous sensing. This work develops a novel coherent receiver of frequency shift keying (FSK) modulation for the bistatic scatter radio channel. The optimal maximum likelihood (ML) coherent detector as well as a simple channel estimation procedure are offered and closed form expressions for the error rate performance of the coherent detector are provided. Additional range gains are achieved by proposing specific short block-length cyclic channel codes. The proposed approach requires minimum encoding complexity, ideal for resource-constrained ultra-low power microcontroller unit (MCU)-based scatter radio tags, adheres to simple low-complexity decoding at the receiver and achieves high-order signal diversity through appropriate low-complexity preprocessing. It is found that the proposed coherent receiver offers up to 4.6dB gain compared to state-of-the-art noncoherent bistatic receiver while gains up to 18dB are reported by employing specific short-block length channel codes. The theoretical design is followed by experimental validation with a commodity software-defined radio (SDR) reader and custom scatter radio tags; tag-to-reader ranges up to 150 meters are demonstrated with as little as 20mW transmission power, increasing sensing ranges by 10 additional meters compared to the uncoded noncoherent case. With the imminent emergence of backscatter sensor networks as a key element of ubiquitous sensing, this work serves as a small step forward towards the realization of ultra low-cost, low-power, increased range backscatter sensor networks and applications.*

Thesis Supervisor: Associate Professor Aggelos Bletsas

This Page Intentionally Left Blank

## Acknowledgements

I would like to take this opportunity to wholeheartedly thank my advisor, professors, colleagues, family and dear friends. This thesis was made possible only through the support and guidance they offered.

I would like to extend my sincerest thanks to my advisor and mentor Aggelos Bletsas, who has offered me all the guidance I needed and facilitated my growth, both personally and academically, throughout my course as a graduate student. His patience, time and advise is precious to me.

Special thanks are also due to my excellent professors and colleagues. Specifically, I would like to thank professors Athanasios P. Liavas and Georgios N. Karystinos who jointly introduced me to the world of communication theory and who helped me to further explore exiting aspects such as optimization theory, information theory and coding theory. I owe Panos N. Alevizos the pleasure of numerous interesting talks and exchange of ideas, many of which shaped this thesis. Emmanouil Alimpertis provided great assistance with the experimental campaigns conducted during this thesis; his technical know-how proved more than valuable. All members of the telecommunication laboratory of the technical university of Crete offered help when needed. Their support is acknowledged.

Finally, I would like to thank my friends and family for the invaluable moral support they provided. My parents, brother and friend Katia Vlachaki deserve mention, although I couldn't possibly write enough.

This work was supported by the ERC-04-BLASE project, executed in the context of the "Education & Lifelong Learning" Operational Program of the National Strategic Reference Framework (NSRF), General Secretariat for Research & Technology (GSRT), funded through European Union-European Social Fund and Greek national funds.

This Page Intentionally Left Blank

# Contents

<b>Abstract</b>	<b>1</b>
<b>Acknowledgements</b>	<b>1</b>
<b>1 Introduction</b>	<b>1</b>
1.1 Communication by Means of Reflection . . . . .	1
1.2 Thesis Contributions . . . . .	5
1.3 Mathematical Notation . . . . .	7
<b>2 Coherent Receiver for Bistatic Scatter Radio Links</b>	<b>9</b>
2.1 Signal Model and Modulation Scheme . . . . .	9
2.2 Noncoherent Detection for Bistatic FSK Modulation . . . . .	13
2.3 ML Coherent Detection for Bistatic FSK Modulation . . . . .	16
2.3.1 Decision Rule and Error Performance . . . . .	16
2.3.2 Joint Channel - Phase Estimation with Least Squares . . . . .	17
2.4 BER performance . . . . .	19
<b>3 Channel Codes and Signal Diversity</b>	<b>21</b>
3.1 Why Channel Codes? . . . . .	21
3.2 Linear and Cyclic Block Codes . . . . .	22
3.2.1 The $\mathcal{G}(23, 12)$ Golay and $\mathcal{C}(31, 11)$ BCH Code . . . . .	27
3.3 Encoding & ML Decoding for Block-coded Bistatic FSK . . . . .	28
3.4 Signal Diversity through Coding . . . . .	30
3.5 BER performance . . . . .	32

<b>4</b>	<b>Performance</b>	<b>37</b>
4.1	Probability of Error for Coherent Bistatic FSK . . . . .	37
4.1.1	Conditional Probability of Error . . . . .	37
4.1.2	Probability of Error . . . . .	37
4.2	Experimental Results: Achieved Bistatic Ranges . . . . .	40
4.2.1	Scenario 1: Uncoded Bistatic Binary FSK . . . . .	41
4.2.2	Scenario 2: Coded Bistatic Binary FSK . . . . .	42
<b>5</b>	<b>Conclusions</b>	<b>45</b>
5.1	Conclusions . . . . .	45
5.2	Future Work . . . . .	46
<b>6</b>	<b>Appendix</b>	<b>49</b>
6.1	Independence of Projected Noise Components . . . . .	49
6.2	Derivative of $Q$ Function . . . . .	50
	<b>Bibliography</b>	<b>53</b>

# List of Figures

1.1	Scatter radio architectures can be either monostatic {I, II} or bistatic {III}. In monostatic architectures the transmit antenna generating the carrier sinusoid as well as receive antenna for demodulating reflected signal are part of the same equipment. In bistatic architectures, the carrier signal generator is detached, potentially decreasing tag-emitter distances thus offering link budget gains. . . . .	2
1.2	Bistatic scatter radio architecture - Multiple ultra-low cost tags, equipped with sensing capabilities, are spread in an area. Carrier emitters are placed to illuminate the tags/sensors, forming backscatter cells. The reflected information is collected and processed centrally by a reader. . . . .	4
2.1	Bistatic architecture system model: the carrier emitter is displaced from the SDR reader and the scatter radio tag modulates the incident RF signal from the carrier emitter. . . . .	10
2.2	The structure of the noncoherent correlation receiver with $M = 4$ correlators.	15
2.3	The structure of the coherent correlation receiver with $M = 4$ correlators. . .	16
2.4	Bit error rate (BER) performance as a function of the average received SNR for the bistatic setup, with coherent and noncoherent receivers. Perfect channel state information (CSI) is assumed available for coherent reception.	19
2.5	Bit error rate (BER) performance as a function of the average received SNR for the bistatic setup, with coherent and noncoherent receivers. The coherent receiver utilizes the LS approach of Eq. <b>2.32</b> . . . . .	20

3.1	Shift register encoder for cyclic codes: The memory elements are initialized with zeros and the message sequence $m(x)$ is given as input (first element first) followed by $n - k$ zeros. During each clock tick, the coded bits are output (first element first). Switches are active if $g_i = 1$ , $i = 0 \dots n - k$ . . . . .	25
3.2	Encoding in ultra-low power, micro-controller unit (MCU)-based tags can be performed with a shift register encoder. . . . .	28
3.3	The structure of the coherent correlation decoder. The vector representations of $n$ signals (one for each coded bit) are passed to the decoder. The decoder infers the transmitted codeword by selecting the most likely codeword (in the ML sense). . . . .	29
3.4	Matrix (block) interleaver: the tag stores a block of $D$ codewords in a $D \times n$ matrix and the information is transmitted column-wise. This way, fading affects bits of different codewords rather than consecutive bits of the same codeword. . . . .	31
3.5	BER performance as a function of the average received SNR for uncoded noncoherent detection, uncoded coherent detection and coherent decoding with the Golay $\mathcal{G}(23, 12)$ and BCH $\mathcal{C}(31, 11)$ codes. A transmission budget is assumed, which spreads the available energy over the coded bits. . . . .	33
3.6	BER performance as a function of the average received SNR. Both uncoded noncoherent and coherent detection are considered as well as coherent decoding by Eq. <b>3.15</b> for the Golay $\mathcal{G}(23, 12)$ code and various interleaving depths $D$ . . . . .	34
3.7	BER performance as a function of the average received SNR. Both uncoded noncoherent and coherent detection are considered as well as coherent decoding by Eq. <b>3.15</b> for the BCH $\mathcal{C}(31, 11)$ code and various interleaving depths $D$ . . . . .	35
4.1	Bistatic experimental setup - The carrier emitter, RF tag and software-defined radio are placed on an open field. The distance between carrier emitter and RF tag is set to $d_{CT} = 10\text{m}$ . . . . .	40

4.2	Right- Experimental bit error rate (BER) for noncoherent detection and ML coherent detection as a function of the tag-to-reader distance. Left- Simulated BER performance as a function of the average received SNR under Ricean block-fading. . . . .	41
4.3	Right- Experimental bit error rate (BER) for noncoherent detection, ML coherent detection and ML decoding as a function of the tag-to-reader distance. Left- Simulated BER performance as a function of the average received SNR under Ricean block-fading. . . . .	43
4.4	Custom carrier emitter, semi-passive scatter radio tag and a commodity SDR.	43
5.1	Challenge 1 - Exploiting joint source channel coding (JSCC) techniques to improve the system's performance. . . . .	46
5.2	Challenge 2 - RSS-based tag localization with multiple emitters and signals measured directly at the reader. . . . .	47
5.3	Challenge 3 - Designing a receiver to account for backscattered tag signals reflected by adjacent tags. . . . .	48

This Page Intentionally Left Blank

# Introduction

## 1.1 Communication by Means of Reflection

Dramatic advances in sensor technology are driving the ubiquitous deployment of large-scale wireless sensor networks (WSNs) to unprecedented levels. Current state-of-the-art WSNs have been seemingly integrated into many aspects of every-day life and are constantly deployed for a plethora of monitoring and/or control applications in some of the most diverse fields [2]. One of the most promising applications of WSNs is that of environmental monitoring, where literally hundreds or thousands of sensors are deployed to monitor various environmental variables at scales and resolutions previously considered impossible to achieve. The dream of ubiquitous large-scale sensing generates increased demands for scalability, prolonged network lifetime and reduced monetary cost, challenging existing WSN technologies to adapt under strict budgets or limited energy resources.

Scatter radio, i.e communications by means of reflection [24], although dating back to 1948, has only recently emerged as a potential key-enabling technology for ubiquitous sensing. Scatter radio has been extensively utilized in radio frequency identification (RFID) systems for supply chain monitoring and object tracking. Rapid advances in sensor technology and the evolution of RFID systems has facilitated the integration of low-cost sensors with RFID technology [28], giving rise to a new generation of low-cost and low-power WSNs that deviate from conventional sensor network wisdom.

Scatter radio achieves this by centrally generating a carrier wave that is used to simultaneously illuminate *multiple* tags/sensors. The tags/sensors do not actively radiate power but instead rely on the principle of *reflecting* the carrier induced incident RF signal

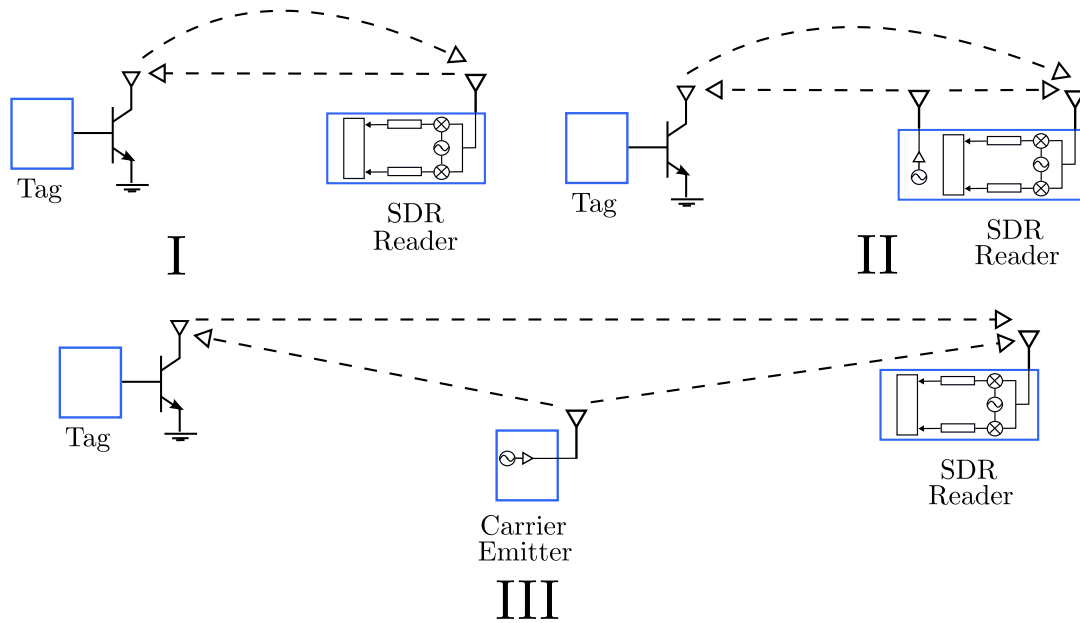


Figure 1.1: Scatter radio architectures can be either monostatic {I,II} or bistatic {III}. In monostatic architectures the transmit antenna generating the carrier sinusoid as well as receive antenna for demodulating reflected signal are part of the same equipment. In bistatic architectures, the carrier signal generator is detached, potentially decreasing tag-emitter distances thus offering link budget gains.

by altering the physical properties of an antenna in a way that depends upon the data sensed. The latter can be viewed as the modulation process, and the reflected signal is subsequently captured by a reader for demodulation and detection. The benefit of such approach lies in the fact that the scatter radio tags adhere to simpler designs, essentially consisting of a single radio frequency (RF) transistor front-end. This way, both monetary cost and energy requirements can be kept at relatively low levels, enabling dense large-scale sensor deployments that overcome many of the issues associated with conventional WSN systems.

Commercial RFID readers and passive (battery-less) tags/sensors typically lie at the heart of existing scatter radio sensing testbeds. Monostatic architectures are usually employed (Fig. 1.1-{I, II}), where the transmit antenna generating the carrier sinusoid as well as receive antenna for demodulating reflected signal are part of the same equipment. Either a single antenna is used for transmission and reception, as depicted in Fig. 1.1-{I} or two different antennas are used for transmission and reception as in Fig. 1.1-{II}.

The main drawback of monostatic architectures is the severe impact of the round-trip path loss. While the tag design is significantly simplified, the carrier signal needs to propagate from the reader to the tag and subsequently be reflected back. This means that received signal-to-noise ratio (SNR) at the reader drops with the fourth power of reader-to-tag distance, or the eighth power considering a more realistic two-ray propagation model [25].

In conjunction with passive tags, monostatic architectures offer limited communication ranges on the order of a few meters. Significant research focus has been placed on increasing the achievable ranges of scatter radio. Research directions include the use of semi-passive (i.e energy assisted) tags, employing new scatter radio architectures and improving the error performance by utilizing error-correction techniques.

### **Increasing scatter radio range: Semi-passive tags**

Communication ranges can be increased by employing semi-passive (i.e energy-assisted) tags; such tags include a battery [27] or rely on energy harvesting techniques [21], [22] but continue to employ reflection rather than active transmission. This way, larger communication ranges can be achieved.

Using battery-assisted tags, work in [27] proposed a monostatic architecture (as in Fig. 1.1-**{II}**) and offered detection algorithms for non-coherent minimum shift keying (MSK) modulation at the tags. Assuming very small bit rates -sufficient for sensing application where stable environmental conditions are monitored- and hence increased energy per bit, the authors in [27] demonstrated extended tag-reader ranges on the order of 15m in an indoor scenario with as little as 7dBm transmit power.

### **Increasing scatter radio range: Bistatic architectures**

By dislocating the carrier signal generator from the reader, *bistatic* architectures can be employed (Fig. 1.1-**{III}**). Bistatic architectures overcome most of the drawbacks of monostatic architectures by enabling more flexible topologies; multiple low cost carrier emitters can be placed in a given area, each emitter illuminating a different subset of tags (Fig. 1.2). This way, the probability that a tag is placed close to a carrier emitter increases, offering potential link budget gains.

The complete bistatic scatter radio signal model was first derived in [1] utilizing two dig-

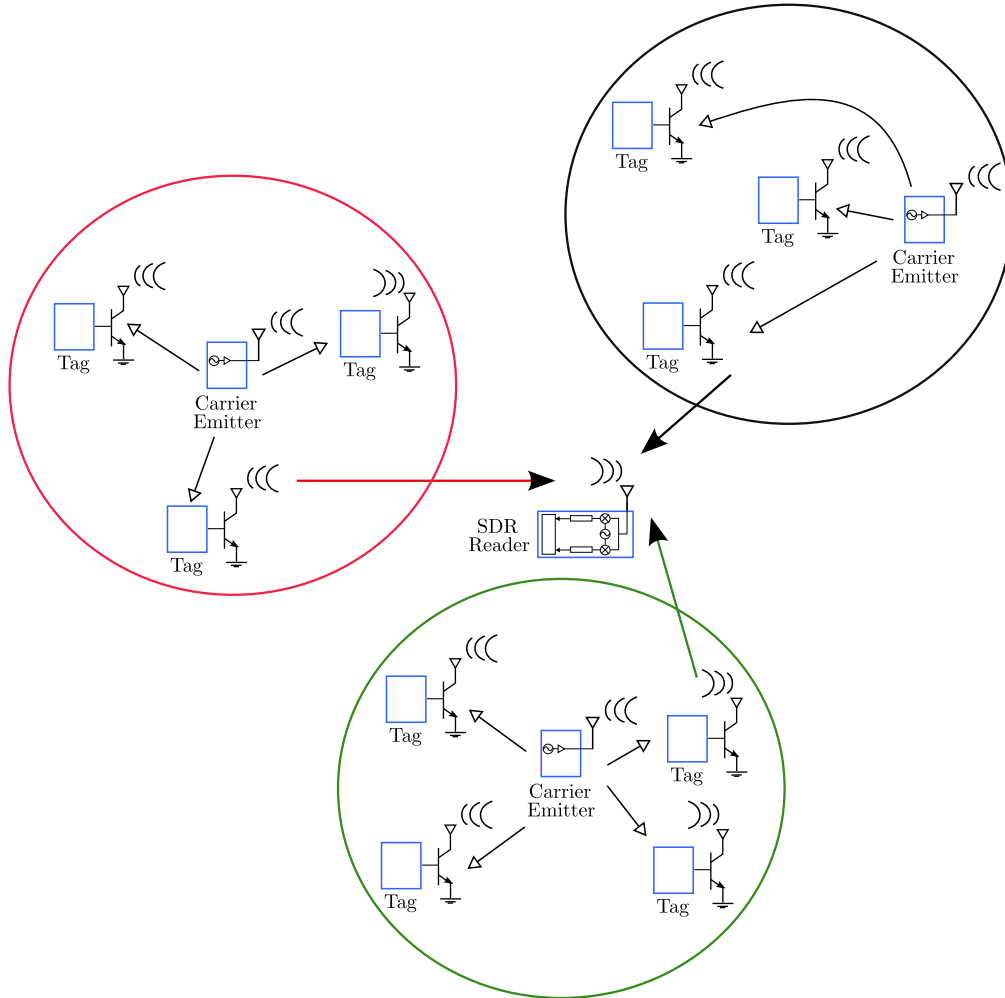


Figure 1.2: Bistatic scatter radio architecture - Multiple ultra-low cost tags, equipped with sensing capabilities, are spread in an area. Carrier emitters are placed to illuminate the tags/sensors, forming backscatter cells. The reflected information is collected and processed centrally by a reader.

ital modulation schemes: on-off keying (typically employed in commercial RFID systems) as well as frequency-shift keying (ideal for the power-limited regime). The authors proposed non-coherent<sup>1</sup> detectors for each modulation scheme and subsequently demonstrated experimental ranges on the order of 100 meters using semi-passive tags in an outdoor scenario with 13dBm transmission power. It is noted that the system model adopted from [1], has been extensively verified experimentally [10–14].

<sup>1</sup> Preliminary work on coherent detection for bistatic on-off keying can be found in [4].

### Increasing scatter radio range: Error-correction coding

An additional approach towards range maximization relies on the use of channel codes (i.e. error-correction coding). A coded system generally introduces *coding gain*, i.e. coded systems achieve a target bit error rate (BER) with smaller receive signal-to-noise ratio (SNR) compared to an uncoded system. Therefore, coded systems offer extended ranges with respect to conventional uncoded systems.

As early as 1948 it was shown that there exist codes which, under certain conditions, exhibit vanishing probability of error as the length of the codewords, i.e. number of bits, goes to infinity. This result single-handedly revolutionized modern communications and generated considerable research effort in the direction of designing practical encoding and decoding algorithms for such large codes.

Noticeable milestones include the invention of Turbo codes [7], low-density parity check (LDPC) codes [20] and the more recent Polar codes [6]. From a practical point of view, scatter radio cannot support such class of codes, due to limited tag processing and storage capabilities; error correction codes of a) *short* codeword length and b) *low-complexity* encoding, appropriate for resource-constrained tags/sensors are strict design options.

Work in [3] first employed channel coding (i.e. error correction) techniques, tailored to the noncoherent bistatic scatter radio setup of [1] to further increase communication ranges. The authors proposed low-complexity (small codeword length) encoding for adding redundancy to the information reflected by the tag; a near-optimal joint detection-decoding procedure was then proposed to exploit such redundancy for improved BER performance at the reader. Experimental results demonstrated range gains of the order of ten or more meters compared to the uncoded setup of [1].

## 1.2 Thesis Contributions

This work further increases range coverage by developing novel *coherent* (instead of noncoherent) receivers for bistatic scatter radio, extending recent work in [1]. Such task may seem formidable since (a) in the bistatic setup signals propagate over three different channels, as opposed to the single communication channel of conventional point-to-point communications and (b) scatter radio further complicates the problem by introducing additional design parameters (such as antenna structural mode, antenna reflection coefficients, scat-

tering efficiency) which are generally unknown at the receiver. Despite the challenging nature of scatter radio, the proposed coherent receiver improves BER performance compared to state-of-the-art noncoherent bistatic receivers and specific analytical, simulation as well as experimental corroborating results are offered.

Furthermore, additional range gains are achieved by proposing specific short block-length cyclic channel codes. The scatter radio tag introduces redundancy to the reflected information (encoding) and the receiver/reader exploits such redundancy to improve BER performance (decoding). The proposed approach requires minimum encoding complexity at the tag (ideal for resource-constrained scatter radio tags), adheres to simple low-complexity decoding at the reader and achieves high-order signal diversity through appropriate low-complexity preprocessing.

More specifically:

- Chapter 2 derives the optimal maximum likelihood (ML) coherent detector for the bistatic scatter radio channel and provides a simple procedure to estimate the channel parameters. The analytical error performance of the system is offered and losses due to imperfect channel estimation are analyzed. The performance gains of the proposed coherent detector are highlighted by simulations.
- Chapter 3 begins by providing a brief overview of finite block length channel codes, proposes specific low-complexity, small codeword-length cyclic block codes and offers the optimal (in the ML sense) decoder. The structure of the specific class of codes is further exploited to perform low-complexity encoding, guaranteed to achieve high-order diversity. Significant performance gains are demonstrated via simulations.
- Chapter 4 provides detailed derivation of the analytical bit-error rate performance for coherent detection of bistatic BFSK modulated signals. Experimental validation of the theoretical design follows with extended tag-reader ranges on the order of 150 meters reported, utilizing as little as 20mW transmission power and omnidirectional antennas. It is experimentally verified that the proposed receivers offer range extension on the order of 10 meters compared to state-of-the-art noncoherent receivers for bistatic scatter radio.
- Chapter 5 concludes the work and provides directions for future research while Chapter 6 serves as the appendix.

## 1.3 Mathematical Notation

Consistent notation is used throughout this thesis, although at times consistency is sacrificed to follow conventions used in the corresponding research literature.

Vectors are denoted by lower case bold Roman letters such as  $\mathbf{x}$ , and all vectors, unless specified otherwise, are assumed to be column vectors. The superscript  $T$  denotes the transpose of a vector, hence a row vector with  $n$  elements is written as  $\mathbf{x}^T = (x_1, \dots, x_n)$  or equivalently as  $\mathbf{x}^T = [x_1 \ \dots \ x_n]$ . The  $i$ -th column of the identity matrix is denoted as  $\mathbf{e}_i$ .

Upper-case bold Roman letters, such as  $\mathbf{C}$ , denote matrices. Matrices are accompanied by a subscript of the form  $k \times m$  which denote the row and column dimensions respectively. Frequently, the dimensions of a matrix will be omitted when clear from context. The  $n \times n$  identity matrix is denoted by  $\mathbf{I}_n$ .

Superscript  $T$  denotes the transpose of a matrix or vector while superscript  $*$  denotes the element-wise conjugate of a complex matrix or vector. Superscript  $H$  denotes the Hermitian transpose of a matrix or vector, i.e the result of first transposing the matrix or vector and then conjugating it.

Notation  $p_x(x)$  is used to denote the probability density function (p.d.f) of random variable  $x$ . Subscript  $x$  is usually omitted to keep notation uncluttered hence the p.d.f of r.v  $x$  is denoted simply as  $p(x)$ .

Symbol  $\Re\{\cdot\}$  is used to denote the real part of a complex scalar or vector, while  $\Im\{\cdot\}$  denotes the imaginary part of a complex scalar or vector.



# Coherent Receiver for Bistatic Scatter Radio Links

## 2.1 Signal Model and Modulation Scheme

The bistatic scatter radio architecture is employed [1], with a carrier emitter, a sensor tag and a software-defined radio (SDR), as depicted in Fig. 2.1. In contrast to conventional monostatic RFID systems, the carrier emitter is dislocated from SDR reader and transmits a carrier at the ultra high frequency (UHF) band, illuminating a tag. The latter modulates the received carrier by terminating its antenna between two different loads (for binary modulation);<sup>1</sup> the incident sinusoid wave is reflected with changed phase and amplitude, depending on the tag antenna load selected each time.

Due to the relatively small communication bandwidth, i.e low bit rate sensing applications, frequency non-selective fading is assumed. Assuming slow fading, the baseband channel response for each of three links depicted in Fig. 2.1 during the channel coherence time,  $T_{coh}$ , is given by:

$$\begin{aligned} h_{CT} &= a_{CT}e^{-j\phi_{CT}}, \\ h_{TR} &= a_{TR}e^{-j\phi_{TR}}, \\ h_{CR} &= a_{CR}e^{-j\phi_{CR}}, \end{aligned} \tag{2.1}$$

where  $a_{CT}, a_{TR}, a_{CR} \in \mathbb{R}_+$  denote the channel attenuation parameters and  $\phi_{CT}, \phi_{TR}, \phi_{CR} \in$

---

<sup>1</sup>Utilization of  $M \geq 2$  loads for  $M$ -ary modulation was recently demonstrated in [26].

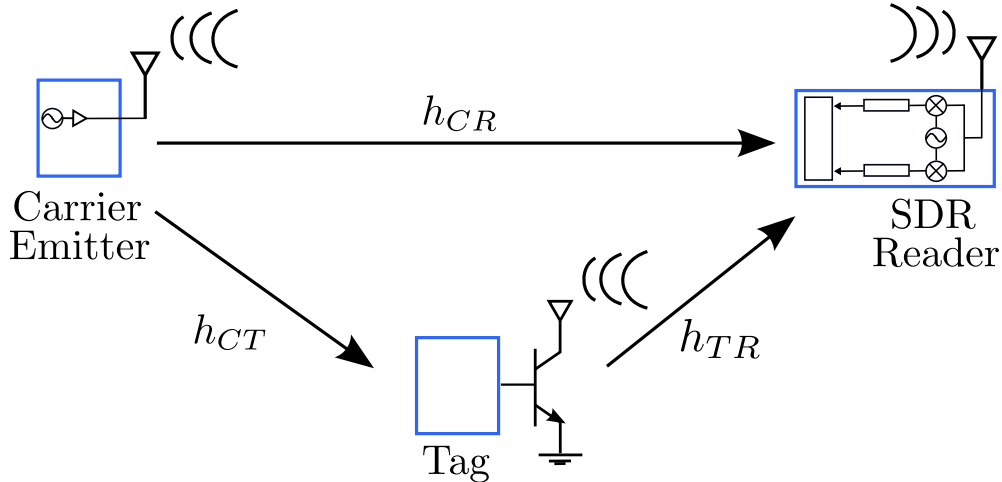


Figure 2.1: Bistatic architecture system model: the carrier emitter is displaced from the SDR reader and the scatter radio tag modulates the incident RF signal from the carrier emitter.

$(0, 2\pi)$  denote the corresponding phases due to the signal propagation delay.

The channel attenuation parameters are assumed Rayleigh distributed and the corresponding phases are assumed uniformly distributed in the interval  $[0, 2\pi)$ . The channel parameters are independent of each other and change independently every  $T_{coh}$ .

The carrier emitter transmits a continuous sinusoid wave of frequency  $F_c$ ; its complex baseband equivalent is given by:

$$c(t) = \sqrt{2P_c}e^{-j(2\pi\Delta Ft + \Delta\phi)}, \quad 2.2$$

where  $\Delta F$  and  $\Delta\phi$  model the frequency and phase offset between the carrier emitter and the SDR respectively, while  $P_c$  denotes the carrier transmission power.

The tag is illuminated by the sinusoid wave  $c(t)$ , attenuated and rotated due to the channel gain  $h_{CT}$ . Modulation is then performed at the tag by switching its antenna between two distinct values (and thus, producing two distinct reflection coefficients  $\Gamma_0$  and  $\Gamma_1$ ) with different rates  $F_0$  and  $F_1$  (with  $F_0$  corresponding to bit 0 and  $F_1$  to bit 1). The reflected modulated waveform is further attenuated by a constant  $s$ , which depends on the tag inherent scattering efficiency. More specifically, the baseband scattered waveform can be written as [1]:

$$x(t) = su_i(t)a_{CT}e^{-j\phi_{CT}}c(t), \quad i \in \{0, 1\}. \quad 2.3$$

For FSK modulation and limited receiver bandwidth  $W \ll 3F_i$ , waveform  $u_i(t)$  - corresponding to bit  $b_i \in \{0, 1\}$ - represents the fundamental frequency component of a 50% duty cycle square waveform of frequency  $F_i$  and random initial phase  $\Phi_i \in [0, 2\pi)$ :

$$u_i(t) = u_0 + \frac{\Gamma_0 - \Gamma_1}{2} \frac{4}{\pi} \cos(2\pi F_i t + \Phi_i), \quad i \in \{0, 1\}, \quad 2.4$$

where  $u_0$  is a constant depending on the tag antenna structural mode  $A_s$  and the tag reflection coefficients  $\Gamma_0, \Gamma_1$  [8].

For duration  $T$  of a single bit  $b_i \in \{0, 1\}$ , the received demodulated signal at the SDR is given by the superposition of the carrier emitter sinusoid and the backscattered tag signal through channels  $h_{CR}$  and  $h_{TR}$ :

$$y(t) = a_{CR} e^{-j\phi_{CR}} c(t) + a_{TR} e^{-j\phi_{TR}} x(t) + n(t), \quad 2.5$$

where  $n(t)$  denotes complex low-pass additive Gaussian noise with power spectral density (PSD):

$$S_{nn}(F) = \begin{cases} \frac{N_0}{2}, & |F| \leq W \\ 0, & \text{otherwise} \end{cases} \quad 2.6$$

By substituting Eqs. 2.2-2.4 in Eq. 2.5, the received baseband signal at the SDR for duration  $T$  of a single bit  $b_i \in \{0, 1\}$  can be written as:

$$y(t) = \underbrace{\left( \sqrt{2P_c} (a_{CR} e^{-j(\phi_{CR} + \Delta\phi)} + s u_0 e^{-j(\phi_{CT} + \phi_{TR} + \Delta\phi)}) \right)}_{\text{DC term}} + m_{CTR} e^{-j\phi_{CTR}} \cos(2\pi F_i t + \Phi_i) \times e^{-j2\pi\Delta F t} + n(t), \quad 2.7$$

where for simplified notation:

$$\begin{aligned} \phi_{CTR} &= \phi_{CT} + \phi_{TR} + \Delta\phi + \angle(\Gamma_0 - \Gamma_1), \\ m_{CTR} &= \sqrt{2P_c} |\Gamma_0 - \Gamma_1| a_{CT} a_{TR} \frac{2}{\pi}. \end{aligned} \quad 2.8$$

The carrier frequency offset (CFO) can be directly estimated using standard periodogram-based estimation techniques, as in [1]. Assuming perfect CFO estimate  $\hat{\Delta F}$ , the received signal can be compensated by multiplying the received signal of Eq. 2.7 with  $e^{j2\pi\hat{\Delta F}t}$ .

The DC term does not contribute any information and hence can be eliminated with a DC-blocking filter. The latter can be accomplished by estimation and removal of the received signal's mean value  $\mathbb{E}\{y(t)\}$ .

After CFO compensation and DC-blocking, the received signal waveform over one bit period  $T$  is given by:

$$y(t) = h_{CTR} \cos(2\pi F_i t + \Phi_i) + n(t) \quad 2.9$$

or equivalently, by:

$$y(t) = \frac{h_{CTR}}{2} \left( e^{j(2\pi F_i t + \Phi_i)} + e^{-j(2\pi F_i t + \Phi_i)} \right) + n(t), \quad 2.10$$

with

$$h_{CTR} = m_{CTR} e^{-j\phi_{CTR}}. \quad 2.11$$

Eq. 2.10 reveals that because tag modulation occurs directly at passband, *two* subcarriers appear for each frequency  $F_i$ , one at the positive semiaxis ( $F_i$ ) and one at the negative ( $-F_i$ ). In contrast, for a classic FSK transmitter, only one subcarrier appears for each frequency and the optimum FSK receiver correlates the received signal against frequencies  $F_0$  and  $F_1$  for signal detection [19] (pp. 178). If the same receiver is utilized for bistatic FSK, the subcarriers at frequencies  $-F_0$  and  $-F_1$  are not considered resulting in a 3dB loss of performance [1]. Evidently, a classic FSK receiver is not directly applicable in scatter radio.

The *instantaneous* received signal-to-noise ratio per bit is defined as:

$$\overline{\text{SNR}} \triangleq \frac{\mathbb{E}\{E_b\}}{N_0/2} = \frac{(8/\pi^2)|\Gamma_0 - \Gamma_1|^2 s^2 P_C (a_{CT})^2 (a_{TR})^2 T}{N_0}, \quad 2.12$$

where  $E_b$  is the instantaneous energy per bit and  $T$  denotes the nominal bit duration.

The *average* received SNR is then defined as:

$$\overline{\text{SNR}} \triangleq \frac{\mathbb{E}\{E_b\}}{N_0/2} = \frac{(8/\pi^2)|\Gamma_0 - \Gamma_1|^2 s^2 P_C \mathbb{E}\{(a_{CT})^2\} \mathbb{E}\{(a_{TR})^2\} T}{N_0}. \quad 2.13$$

For Rayleigh fading

$$a_x \sim |\mathcal{CN}(0, \sigma_x^2)| \implies \mathbb{E}\{(a_x)^2\} = \sigma_x^2, \quad x \in \{CR, CT, TR\}, \quad 2.14$$

hence the average received SNR is given by:

$$\overline{\text{SNR}} = \frac{(8/\pi^2)|\Gamma_0 - \Gamma_1|^2 s^2 P_C \sigma_{CT}^2 \sigma_{TR}^2 T}{N_0}. \quad 2.15$$

## 2.2 Noncoherent Detection for Bistatic FSK Modulation

The received signal of Eq. 2.9 is the sum of two complex exponentials of frequencies  $\pm F_i$  and unknown phases ( $\pm\Phi_i - \phi_{CTR}$ ),  $i \in \{0, 1\}$ . If the orthogonality criterion for non-coherent FSK is satisfied, i.e:

$$|F_1 - F_0| = \frac{k}{T}, \quad k \in \mathbb{N}, \quad 2.16$$

where  $T$  denotes the nominal bit duration, any two exponentials of frequencies  $\pm F_0, \pm F_1$  will be orthogonal [1]:

$$\begin{aligned} \langle e^{\pm j2\pi(F_i)t}, e^{\pm j2\pi(F_k)t} \rangle &\triangleq \int_T e^{\pm j2\pi(F_i)t} (e^{\pm j2\pi(F_k)t})^* dt \\ &= \int_T e^{\pm j2\pi(F_i - F_k)t} dt \\ &= \begin{cases} T, & F_i = F_k, \\ 0, & F_i \neq F_k, \end{cases}, \quad k, i \in \{0, 1\}, \end{aligned} \quad 2.17$$

where the subscript  $T$  in the integral denotes that integration is performed over one bit period. Consequently, the set of exponentials of frequencies  $\pm F_0, \pm F_1$ , normalized by  $\sqrt{T}$ , constitute an orthonormal basis [19] that can be used for expansion of the received signal of Eq. 2.9. It is further noted that for  $1 \ll WT$  the basis functions are limited within the  $[-W, W]$  frequency range.

Utilizing the orthonormal set, the vector equivalent of the received signal for duration  $T$  of a single bit  $b_i \in \{0, 1\}$  is given by:

$$\mathbf{r} = \mathbf{h} \odot \mathbf{s}_i + \mathbf{n}, \quad 2.18$$

with elements:

$$\begin{bmatrix} r_0^+ \\ r_0^- \\ r_1^+ \\ r_1^- \end{bmatrix} = \begin{bmatrix} \frac{\sqrt{T}h_{CTR}}{2} e^{+j\Phi_0} \\ \frac{\sqrt{T}h_{CTR}}{2} e^{-j\Phi_0} \\ \frac{\sqrt{T}h_{CTR}}{2} e^{+j\Phi_1} \\ \frac{\sqrt{T}h_{CTR}}{2} e^{-j\Phi_1} \end{bmatrix} \odot \begin{bmatrix} (1 - b_i) \\ (1 - b_i) \\ b_i \\ b_i \end{bmatrix} + \begin{bmatrix} n_0^+ \\ n_0^- \\ n_1^+ \\ n_1^- \end{bmatrix}, \quad 2.19$$

where  $\odot$  denotes the component-wise (Hadamard) product.

To see this, note that the noiseless random process  $s(t, \Phi_i, h_{CTR}) = h_{CTR} \cos(2\pi F_i t + \Phi_i)$  of Eq. 2.9 can be expanded as:

$$\begin{aligned}
 \left\langle s(t, \Phi_i, h_{CTR}), \frac{1}{\sqrt{T}} e^{+j2\pi F_0 t} \right\rangle &= \\
 &= \int_T h_{CTR} \cos(2\pi F_i t + \Phi_i) \left( \frac{1}{\sqrt{T}} e^{+j2\pi F_0 t} \right)^* dt \\
 &= \int_T \frac{h_{CTR}}{2\sqrt{T}} \left( e^{j(2\pi F_i t + \Phi_i)} + e^{-j(2\pi F_i t + \Phi_i)} \right) \left( e^{-j2\pi F_0 t} \right) dt \\
 &= \int_T \frac{h_{CTR}}{2\sqrt{T}} e^{j(2\pi(F_i - F_0)t + \Phi_i)} dt,
 \end{aligned}$$

where the last relation follows from the fact that the integral of the “fast” exponential with frequency  $F_i + F_0$  is approximated by zero. Hence:

$$\begin{aligned}
 \left\langle s(t, \Phi_i, h_{CTR}), \frac{1}{\sqrt{T}} e^{+j2\pi F_0 t} \right\rangle &= \\
 &= \frac{h_{CTR}}{2\sqrt{T}} e^{+j\Phi_i} \int_T e^{j2\pi(F_i - F_0)t} dt = \frac{\sqrt{T} h_{CTR}}{2} e^{+j\Phi_0} (1 - b_i),
 \end{aligned} \tag{2.20}$$

where in the last equality, orthogonality is exploited.

Similarly, using the remaining basis functions :

$$\begin{aligned}
 \left\langle s(t, \Phi_i, h_{CTR}), \frac{1}{\sqrt{T}} e^{-j2\pi F_0 t} \right\rangle &= \frac{\sqrt{T} h_{CTR}}{2} e^{-j\Phi_0} (1 - b_i), \\
 \left\langle s(t, \Phi_i, h_{CTR}), \frac{1}{\sqrt{T}} e^{+j2\pi F_1 t} \right\rangle &= \frac{\sqrt{T} h_{CTR}}{2} e^{+j\Phi_1} b_i, \\
 \left\langle s(t, \Phi_i, h_{CTR}), \frac{1}{\sqrt{T}} e^{-j2\pi F_1 t} \right\rangle &= \frac{\sqrt{T} h_{CTR}}{2} e^{-j\Phi_1} b_i.
 \end{aligned} \tag{2.21}$$

Since  $n(t)$  is a complex baseband Gaussian random process with power spectral density  $\frac{N_0}{2}$  in the  $[-W, W]$  frequency band, its projections on an orthonormal basis (with basis functions limited in the  $[-W, W]$  frequency band) will have i.i.d zero-mean complex Gaussian components with variance  $\frac{N_0}{2}$  (proof given in Appendix):

$$\mathbf{n} = [n_0^+ \ n_0^- \ n_1^+ \ n_1^-]^T \sim \mathcal{CN}\left(0, \frac{N_0}{2} \mathbf{I}_4\right). \tag{2.22}$$

Therefore, when bit  $b_i = 0$  is transmitted the statistics are:

$$\begin{aligned}
 r_0^+ &= \frac{\sqrt{T}}{2} h_{CTR} e^{+j\Phi_0} + n_0^+, & r_1^+ &= n_1^+, \\
 r_0^- &= \frac{\sqrt{T}}{2} h_{CTR} e^{-j\Phi_0} + n_0^-, & r_1^- &= n_1^-,
 \end{aligned}$$

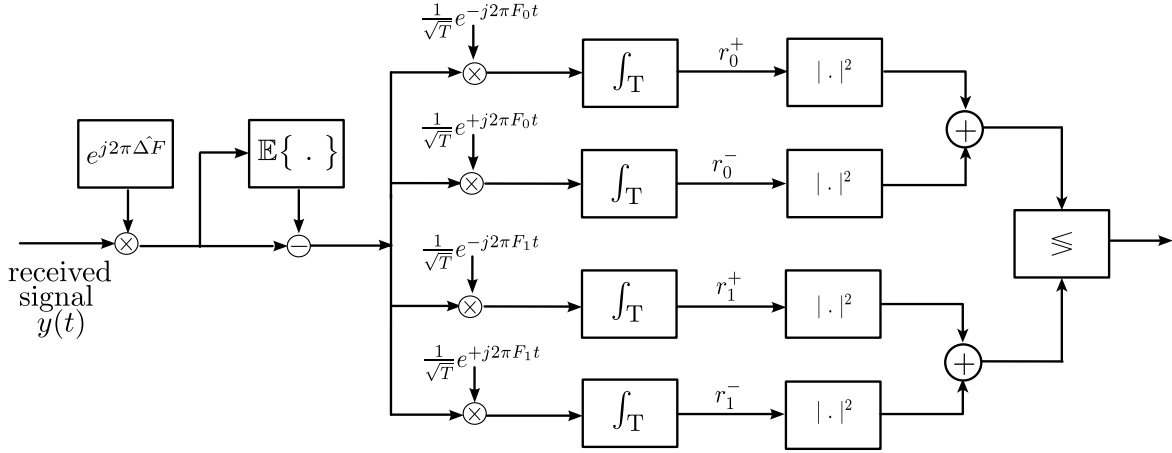


Figure 2.2: The structure of the noncoherent correlation receiver with  $M = 4$  correlators.

while when bit  $b_i = 1$  is transmitted the statistics are:

$$\begin{aligned} r_0^+ &= n_0^+, & r_1^+ &= \frac{\sqrt{T}}{2} h_{CTRE} e^{+j\Phi_1} + n_1^+, \\ r_0^- &= n_0^-, & r_1^- &= \frac{\sqrt{T}}{2} h_{CTRE} e^{-j\Phi_1} + n_1^-. \end{aligned}$$

For noncoherent detection and equiprobable signals, the optimal (in the sense of minimizing the probability of error) detection rule is given by:

$$\begin{aligned} b_i^{ML} &= \operatorname{argmax}_{b_i \in \{0,1\}} p(\mathbf{r}|\mathbf{s}_i) \\ &= \operatorname{argmax}_{b_i \in \{0,1\}} \int p(\mathbf{r}|\mathbf{s}_i, \mathbf{h}) p(\mathbf{h}) d\mathbf{h}, \end{aligned} \quad \mathbf{2.23}$$

where in the last relation, averaging is performed over random parameter vector  $\mathbf{h}$ .

There exists no closed form solution for the expression of Eq. **2.23**, hence to implement optimal noncoherent detection Eq. **2.23** would need to be evaluated numerically. As a practical alternative, the authors in [1] and [3] instead consider a heuristic approximation to the above detection rule. More specifically:

$$z_0 \triangleq |r_0^+|^2 + |r_0^-|^2 \stackrel{\text{bit } 0}{\geq} |r_1^+|^2 + |r_1^-|^2 \triangleq z_1. \quad \mathbf{2.24}$$

The noncoherent receiver is depicted in Fig. 2.2 and employs the above detection rule. Note that the receiver does not require the channel statistics and is solely based on the received information.

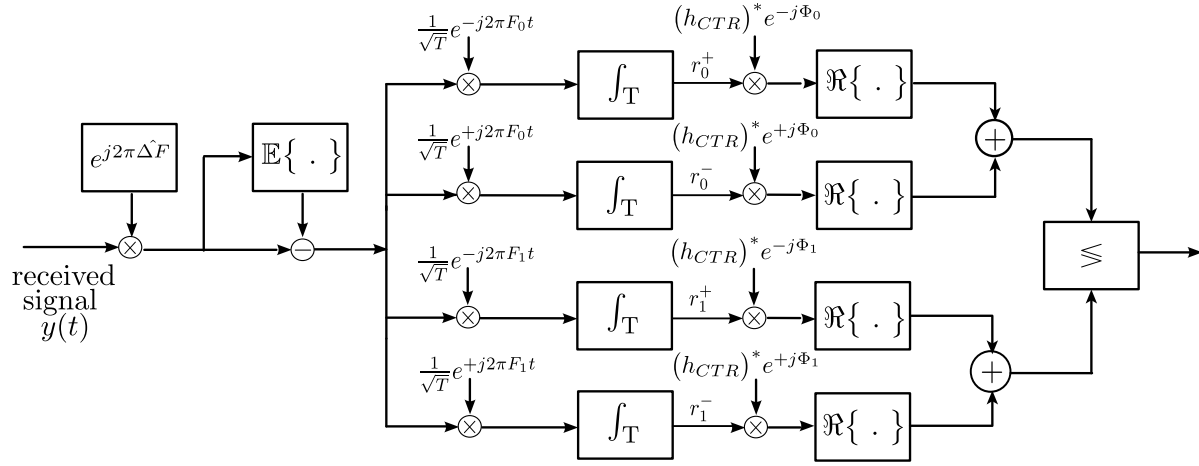


Figure 2.3: The structure of the coherent correlation receiver with  $M = 4$  correlators.

## 2.3 ML Coherent Detection for Bistatic FSK Modulation

### 2.3.1 Decision Rule and Error Performance

Assuming available channel estimate  $\hat{\mathbf{h}}$  and equiprobable signaling, the optimal (in the sense of minimizing the probability of error) detection rule is given by:

$$\begin{aligned}
 b_i^{ML} &= \operatorname{argmax}_{b_i \in \{0,1\}} p(\mathbf{r} | \mathbf{s}_i, \hat{\mathbf{h}}) \\
 &= \operatorname{argmax}_{b_i \in \{0,1\}} \exp \left\{ -\frac{2}{N_0} \|\mathbf{r} - \hat{\mathbf{h}} \odot \mathbf{s}_i\|^2 \right\} \\
 &= \operatorname{argmin}_{b_i \in \{0,1\}} \|\mathbf{r} - \hat{\mathbf{h}} \odot \mathbf{s}_i\|^2 \\
 &= \operatorname{argmin}_{b_i \in \{0,1\}} -\Re \left( (\hat{\mathbf{h}} \odot \mathbf{s}_i)^H \mathbf{r} \right). \tag{2.25}
 \end{aligned}$$

After simple calculations, the optimal decision rule can be written as:

$$\begin{aligned}
 &\Re \left( (\hat{h}_{CTR})^* (e^{-j\hat{\Phi}_0} r_0^+ + e^{+j\hat{\Phi}_0} r_0^-) \right) \stackrel{\text{bit } 0}{\geq} \\
 &\Re \left( (\hat{h}_{CTR})^* (e^{-j\hat{\Phi}_1} r_1^+ + e^{+j\hat{\Phi}_1} r_1^-) \right). \tag{2.26}
 \end{aligned}$$

The coherent receiver is depicted in Fig. 2.3 and employs the above detection rule.

**Lemma 2.1.** The probability of error for coherent detection of bistatic BFSK- modulated signals is given by:

$$\begin{aligned} p(e) &= \mathbb{E}_{\mathbf{h}} \{p(e|\mathbf{h})\} \\ &= \frac{1}{2} - \frac{\sqrt{\pi}}{4} \text{U}\left(\frac{1}{2}, 0, \frac{2}{\text{SNR}}\right), \end{aligned} \quad 2.27$$

where  $\text{U}(a, b, z)$  denotes the *confluent hypergeometric* U function.

*Proof.* Proof given in Chapter 4. ■

### 2.3.2 Joint Channel - Phase Estimation with Least Squares

To coherently detect the received signal by Eq. 2.26, both the compound channel  $h_{CTR}$  as well as the random phases  $\Phi_i$ ,  $i \in \{0, 1\}$  need to be estimated.

One approach favored in practice is to use a special a-priori known signal, called a *pilot* or *training* signal, which serves as a means to measure the channel characteristics. Such approach is followed in this work, where a training signal is periodically transmitted and the receiver then employs an optimization procedure based on least squares (LS), extracting the estimates for the unknown parameters.

More specifically, once during the channel coherence time  $T_{coh}$  - during which the channel characteristics are considered constant - a training signal comprised of  $N_{tr}$  training bits  $\{b_{i_{tr}}\}$ ,  $i_{tr} = 1, \dots, N_{tr}$ , is transmitted by the tag. After demodulation, CFO estimation and DC blocking, the vector representation of the received training signal over one bit period  $T$  is given by Eq. 2.18 as:

$$\mathbf{r}_{i_{tr}} = \mathbf{h} \odot \mathbf{s}_{i_{tr}} + \mathbf{n}_{i_{tr}} \quad 2.28$$

which can also be written as

$$\mathbf{r}_{i_{tr}} = \mathbf{V}_{i_{tr}} \mathbf{h} + \mathbf{n}_{i_{tr}}, \quad \{\mathbf{r}_{i_{tr}}, \mathbf{n}_{i_{tr}}\} \in \mathbb{C}^4, \quad 2.29$$

with

$$\mathbf{V}_{i_{tr}} = \begin{bmatrix} (1 - b_{i_{tr}})\mathbf{e}_1 & (1 - b_{i_{tr}})\mathbf{e}_2 & b_{i_{tr}}\mathbf{e}_3 & b_{i_{tr}}\mathbf{e}_4 \end{bmatrix} \in \mathbb{C}^{4 \times 4}. \quad 2.30$$

where  $\mathbf{e}_k$ ,  $k = 1, \dots, 4$  denotes the  $k$ -th column of the  $\mathbf{I}_4$  identity matrix.

Next, by the column-wise concatenation of the vector representations of the  $N_{tr}$  bits in the training sequence, the receiver creates vector  $\mathbf{y} \in \mathbb{C}^{4N_{tr}}$ :

$$\mathbf{y} = \begin{bmatrix} \mathbf{r}_1 \\ \mathbf{r}_2 \\ \vdots \\ \mathbf{r}_{N_{tr}} \end{bmatrix} = \begin{bmatrix} \mathbf{V}_1 \\ \mathbf{V}_2 \\ \vdots \\ \mathbf{V}_{N_{tr}} \end{bmatrix} \mathbf{h} + \begin{bmatrix} \mathbf{n}_1 \\ \mathbf{n}_2 \\ \vdots \\ \mathbf{n}_{N_{tr}} \end{bmatrix} = \mathbf{A}\mathbf{h} + \mathbf{n}. \quad 2.31$$

To jointly estimate the compound channel  $h_{CTR}$  and phases  $\Phi_i, i \in \{0, 1\}$  the receiver solves the least squares problem

$$\frac{\sqrt{T} \widehat{h}_{CTR}}{2} \begin{bmatrix} e^{+j\widehat{\Phi}_0} \\ e^{-j\widehat{\Phi}_0} \\ e^{+j\widehat{\Phi}_1} \\ e^{-j\widehat{\Phi}_1} \end{bmatrix} = \widehat{\mathbf{h}} \triangleq \mathbf{h}^{LS} = \underset{\mathbf{h} \in \mathbb{C}^4}{\operatorname{argmin}} \|\mathbf{y} - \mathbf{A}\mathbf{h}\|_2^2, \quad 2.32$$

It is noted that while the aforementioned LS approach ignores the dependencies in vector  $\mathbf{h}$ , it adheres to a simple non-iterative solution. Problem 2.32 can be written as:

$$\begin{aligned} \{\mathbf{h}^{LS}\} &= \underset{\mathbf{h} \in \mathbb{C}^4}{\operatorname{argmin}} (\mathbf{y} - \mathbf{A}\mathbf{h})^H (\mathbf{y} - \mathbf{A}\mathbf{h}) \\ &= \underset{\mathbf{h} \in \mathbb{C}^4}{\operatorname{argmin}} (\mathbf{y}^H \mathbf{y} - \mathbf{y}^H \mathbf{A}\mathbf{h} - \mathbf{h}^H \mathbf{A}^H \mathbf{y} + \mathbf{h}^H \mathbf{A}^H \mathbf{A}\mathbf{h}) \\ &= \underset{\mathbf{h} \in \mathbb{C}^4}{\operatorname{argmin}} (\mathbf{h}^H \mathbf{A}^H \mathbf{A}\mathbf{h} - \mathbf{y}^H \mathbf{A}\mathbf{h} - \mathbf{h}^H \mathbf{A}^H \mathbf{y}), \end{aligned} \quad 2.33$$

where in the last relation, term  $\mathbf{y}^H \mathbf{y}$  has been dropped since it does not contribute to the maximization. The derivative w.r.t  $\mathbf{h}$  is given by:

$$\frac{d}{d\mathbf{h}} (\mathbf{h}^H \mathbf{A}^H \mathbf{A}\mathbf{h} - \mathbf{y}^H \mathbf{A}\mathbf{h} - \mathbf{h}^H \mathbf{A}^H \mathbf{y}) = \mathbf{h}^H (\mathbf{A}^H \mathbf{A}) - \mathbf{y}^H \mathbf{A}. \quad 2.34$$

and setting the derivative to zero offers

$$\mathbf{h}^{LS} = (\mathbf{A}^H \mathbf{A})^{-1} \mathbf{A}^H \mathbf{y}. \quad 2.35$$

After obtaining estimate  $\mathbf{h}^{LS}$ , the receiver employs to decision rule of Eq. 2.26 to perform coherent detection. Imperfect channel estimation via Eq. 2.35 degrades performance compared to perfect channel estimation: such performance losses are quantified in the following subsection.

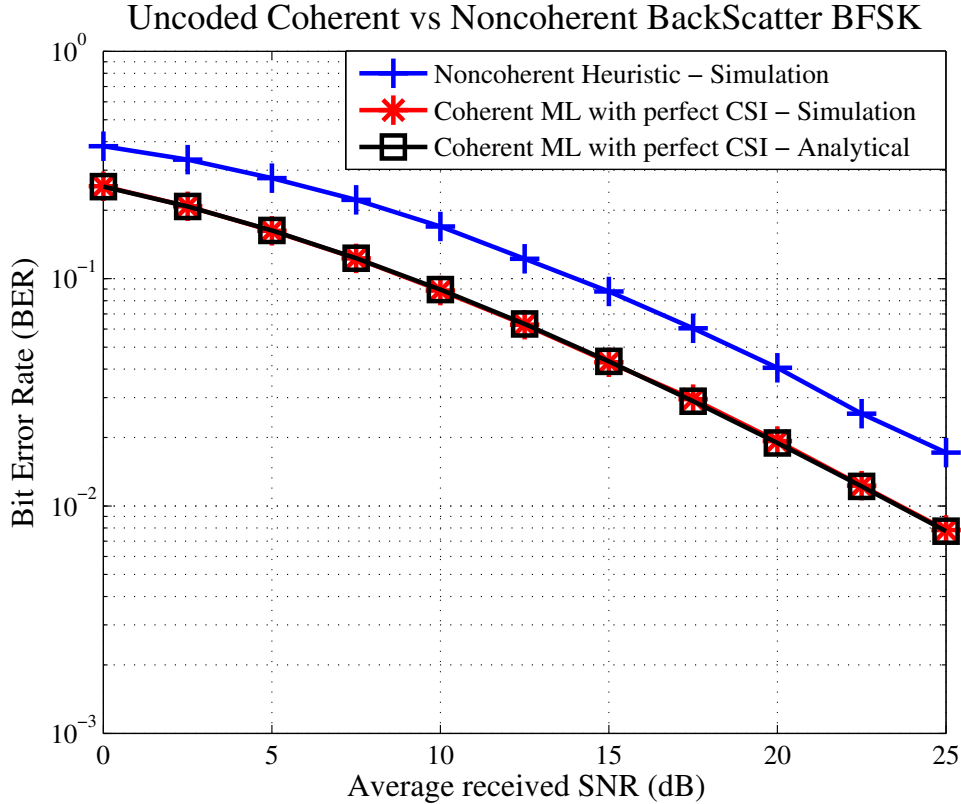


Figure 2.4: Bit error rate (BER) performance as a function of the average received SNR for the bistatic setup, with coherent and noncoherent receivers. Perfect channel state information (CSI) is assumed available for coherent reception.

## 2.4 BER performance

Figs. 2.4–2.5 illustrate the bit error rate (BER) performance as a function of the average received SNR for the bistatic setup of Fig. 2.1, where each channel link is assumed i.i.d Rayleigh distributed with  $\{a_{CT}, a_{TR}, a_{CR}\} \sim |\mathcal{CN}(0, 1)|$ . The channel coherence time is assumed to span a limited number of 200 bits, during which the channel characteristics remain unchanged. During the channel coherence time,  $N_{tr} = 40$  training bits are utilized for solving the LS problem 2.32 and  $N = 160$  bits carry useful information. It is assumed that the receiver synchronizes perfectly using the training bits (as in [1]) and estimates the carrier frequency offset without error.

Both noncoherent detection with Eq. 2.24 and coherent detection with Eq. 2.26 are

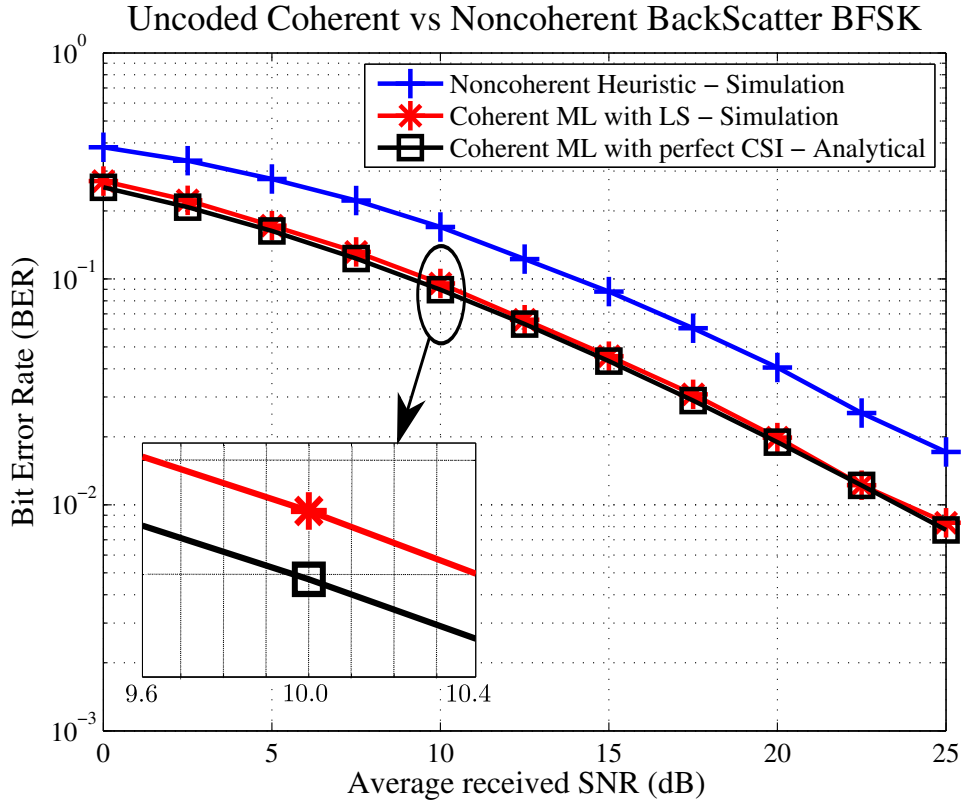


Figure 2.5: Bit error rate (BER) performance as a function of the average received SNR for the bistatic setup, with coherent and noncoherent receivers. The coherent receiver utilizes the LS approach of Eq. 2.32.

considered, following the processing chains of Fig. 2.2 and Fig. 2.3 respectively.

Fig. 2.4 depicts the analytical error rate performance of coherent detection given by Eq. 2.27 as well as the performance of coherent detection assuming perfect channel state information (CSI). It can be seen that analysis BER of Eq. 2.27 perfectly matches with simulation. Evidently, with perfect CSI the coherent detector demonstrates superior bit error rate performance compared to the noncoherent detector with a performance gap of approximately 5dB at  $\text{BER} = 10^{-1}$ . In practice however, the proposed receiver estimates the channel characteristics with the least squares approach of 2.32 and imperfect estimation causes a 0.4dB degradation compared to the theoretical error performance as seen in Fig. 2.5. Therefore, despite estimation errors the proposed receiver offers a 4.6dB performance gain at target  $\text{BER} = 10^{-1}$  compared to the state-of-the-art noncoherent bistatic receiver of [1].

# Channel Codes and Signal Diversity

## 3.1 Why Channel Codes?

Coding, and in particular error-correction coding, is at the heart of communication theory and has revolutionized modern communications. The roots of coding can be traced back to 1948 when Claude E. Shannon published his work on achieving reliable communication over unreliable channels [23]. Shannon formalized the concept of a *code*, defined as a finite set of vectors over some input alphabet. Each one of these vectors has length  $n$  and is referred to as a *codeword*.

For *binary* input alphabets consisting of  $q = 2$  elements (*bits*), there are  $2^n$  possible codewords in a code with length  $n$ . Each codeword however encodes  $k < n$  bits hence only  $2^k$  out of  $2^n$  vectors are actually utilized. In doing so, each of the  $2^k$   $n$ -dimensional vector consists of an additional  $n - k$  bits, referred to as the *redundancy* of the code. The ratio  $k/n$  is called the code rate.

A code is basically a way of transmitting correlated information over an unreliable channel. Therefore, instead of transmitting uncorrelated information, the transmitted information comes in a form of a vector codeword and the underlying correlation is exploited to make tentative decisions about the data. In addition, the added redundancy helps correct any mistakes that occur during transmission.

So assume that a vector codeword is received over an unreliable channel. Such codeword would be corrupted by errors introduced by the channel. The original codeword can be inferred by the observed noisy codeword using a *maximum likelihood decoder*. To perform maximum likelihood decoding, all  $2^k$  possible vector codewords are listed at the receiver side

and the probability of received noisy codeword conditioned on each codeword, is evaluated. The codeword that maximizes the conditional probability is selected as the estimate of the codeword sent. The maximum likelihood decoder is optimal (in the sense of minimizing the decoding error) but takes a lot of time due to the exhaustive search on all possible  $n$ -dimensional codewords, especially if the code is large.

In the context of bistatic scatter radio, application of channel codes is especially challenging due to hard design constraints; scatter radio tags are inherently resource-constrained and thus, any type of processing must be computationally affordable. This means that coding schemes capable of approaching the theoretical limits of performance (capacity approaching codes) are not applicable due to non-negligible encoding complexity. In addition, decoding at the receiver should be also low-complexity; if not, decoding-induced delays would limit the potential number of tags served by a single receiver.

The following section contains a brief overview of the family of *linear block codes* and *cyclic block codes* and examines their applicability for bistatic scatter radio. The focus is subsequently placed on two particular short block-length codes belonging to the class of cyclic block codes, the Golay code and the BCH(31,11) code. The Golay code encodes 12 bits of data into a 23 bit codeword with the BCH(31,11) code encodes 11 bits into 31-bit codewords. The algebraic structure of the codes is exploited to provide efficient encoding at the tag, overcoming limited processing capabilities, while the short code length allows optimal ML decoding with negligible complexity.

## 3.2 Linear and Cyclic Block Codes

To follow the corresponding research literature, vectors are assumed to be row-vectors henceforth i.e  $\mathbf{x} = (x_1 \ x_2 \ \dots \ x_n)$  while column vectors are denoted as  $\mathbf{x}^T$ . All material in this section is based on a combination of [18], [17] and [16]. The interested reader is recommended to consult the corresponding chapters from these excellent references for a detailed treatment of linear and cyclic block codes.

### Linear Block Codes

To set the stage, a *block* code is a code that utilizes sequences of  $n$  symbols, called *codewords*. Each codeword contains  $k$  symbols ( $k < n$ ), called the *information* or *message*

symbols. The remaining  $n - k$  symbols are called *parity-checks symbols*. These symbols contain no useful information, but can be used to correct errors that occur during the transmission of a codeword.

A block code could in essence be represented as an exhaustive list of codewords; information sequences could then be matched directly to their corresponding codewords. However, for large  $k$  this would lead to prohibitive encoding complexity and storage requirements. This complexity can be greatly reduced by imposing mathematical structure to the code, the most common requirement being *linearity*.

A binary block code of length  $n$  and  $2^k$  codewords is a binary *linear* block code if and only if its  $2^k$  codewords form a  $k$ -dimensional vector subspace of the vector space of all binary  $n$ -tuples. The number  $n$  is said to be the *length* of the code and the number  $k$  is the *dimension* of the code. The *rate* of the code is the ratio  $R = k/n$ . The code is denoted as  $\mathcal{C}(n, k)$ .

Since by definition a linear block code is a  $k$ -dimensional vector subspace, there exist  $k$ -linearly independent vectors that generate the vector subspace. In other words, every codeword  $\mathbf{c} \in \mathcal{C}$  can be obtained as a linear combination of these independent vectors. Denoting these vectors as  $\mathbf{g}_0, \mathbf{g}_1, \dots, \mathbf{g}_{k-1}$  each codeword can be represented as:

$$\mathbf{c} = m_0\mathbf{g}_0 + m_1\mathbf{g}_1 + \dots + m_{k-1}\mathbf{g}_{k-1}, \quad \mathbf{3.1}$$

where  $m_i \in \{0, 1\}, i = 0, 1, \dots, k-1$ . Eq. **3.1** can be conveniently represented in matrix form as:

$$\mathbf{c} = [m_0 \ m_1 \ \dots \ m_{k-1}] \begin{bmatrix} \mathbf{g}_0 \\ \mathbf{g}_1 \\ \vdots \\ \mathbf{g}_{k-1} \end{bmatrix} = \mathbf{m}\mathbf{G}. \quad \mathbf{3.2}$$

Hence, an arbitrary linear block code can be specified by a  $(k \times n)$  matrix denoted by  $\mathbf{G}$ , called *generator matrix*. Eq **3.2** is basically the encoding operation for the code  $\mathcal{C}$  that maps binary  $k$ -dimensional vectors  $\mathbf{m}$  to binary  $n$ -dimensional codewords  $\mathbf{c}$ . Due to linearity, representing the code requires storing only  $k$  vectors of length  $n$  as opposed to the  $2^k$  vectors that would be required to store all codewords of a non-linear code.

It can easily be shown [18] that for linear block codes, the linear combination of codewords is a codeword.

## Cyclic Codes

By imposing additional algebraic structure to the code, encoding efficiency can be further improved. Such additional structure can be found in *cyclic* codes, a subset of linear block codes. Cyclic codes are based on polynomial operations, so the discussion on cyclic codes assumes the reader is comfortable with concepts such as polynomial addition, multiplication and division, outlined in [18] (Chapter 4) and [17] (Chapter 8) among others.

An  $(n, k)$  linear code is said to be a *cyclic code* if, for every codeword  $\mathbf{c} = (c_0, c_1, \dots, c_{n-1})$ , the right cyclic shift of  $\mathbf{c}$ , denoted as  $\mathbf{c}^R = (c_{n-1}, c_0, \dots, c_{n-2})$ , is also a codeword. Any vector codeword  $\mathbf{c} = (c_0, c_1, \dots, c_{n-1})$  can be associated with a polynomial  $c(x)$ , defined as:

$$c(x) = c_0 + c_1x + \dots + c_{n-1}x^{n-1}, \quad \mathbf{3.3}$$

with a one-to-one correspondence between vectors and their polynomial representation.

It can easily be shown [17] that if  $\mathbf{c} = (c_0, c_1, \dots, c_{n-1})$  is a codeword with polynomial representation  $c(x) = c_0 + c_1x + \dots + c_{n-1}x^{n-1}$ , then the polynomial representation of the right cyclic shift of  $\mathbf{c}^R$  is given by:

$$c^R(x) = x c(x) \pmod{(x^n - 1)}. \quad \mathbf{3.4}$$

This seemingly unimportant property is extremely useful, as it reveals the additional algebraic structure of the code and is used as the basis for drawing the main conclusions for cyclic codes. For instance, if a codeword polynomial of a cyclic code is multiplied by any other polynomial and the result is reduced mod  $(x^n - 1)$ , the resulting polynomial is also a codeword:

$$\forall c(x) \in \mathcal{C}, \forall p(x) : c'(x) = p(x)c(x) \pmod{(x^n - 1)} \in \mathcal{C}. \quad \mathbf{3.5}$$

To verify this, let  $p(x) = p_0 + p_1x + \dots + p_mx^m = \sum_{i=0}^m p_i x^i$ . Then

$$\begin{aligned} p(x)c(x) \pmod{(x^n - 1)} &= \left( \sum_{i=0}^m p_i x^i \right) c(x) \pmod{(x^n - 1)} \\ &= \sum_{i=0}^m p_i (x^i c(x) \pmod{(x^n - 1)}). \end{aligned}$$

Since the code is cyclic  $x^i c(x) \pmod{(x^n - 1)}$  -i.e right cyclic shifts of  $c(x)$ - is by definition a codeword. Then since the code is linear the linear combination  $\sum_{i=0}^m p_i (x^i c(x) \pmod{(x^n - 1)})$  is a codeword. Hence **3.5** holds.

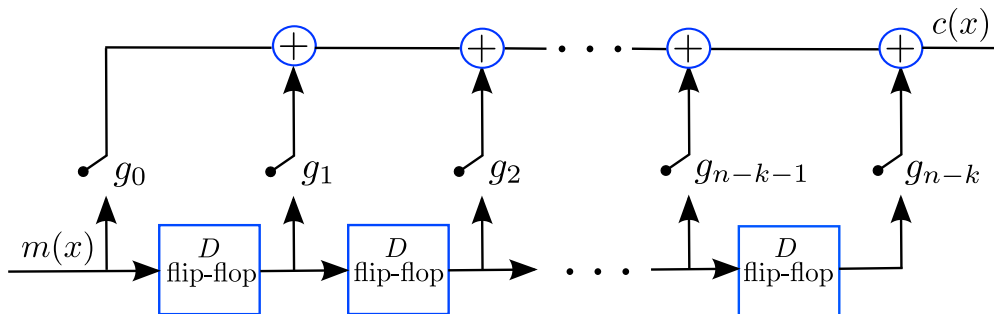


Figure 3.1: Shift register encoder for cyclic codes: The memory elements are initialized with zeros and the message sequence  $m(x)$  is given as input (first element first) followed by  $n - k$  zeros. During each clock tick, the coded bits are output (first element first). Switches are active if  $g_i = 1$ ,  $i = 0 \dots n - k$ .

At the heart of cyclic codes lies the notion of a *generator* polynomial, usually denoted as  $g(x)$  and defined as a nonzero polynomial of minimal degree in  $\mathcal{C}(n, k)$ . It can be shown that the generator polynomial  $g(x)$  of a cyclic code  $\mathcal{C}(n, k)$  is always *unique* up to multiplication by scalars, is monic and is a divisor of  $x^n - 1$  (for details refer to chapter 4 in [18]).

Using all the above, it can be shown that every  $\mathcal{C}(n, k)$  binary cyclic code has a unique minimal monic generator polynomial  $g(x)$  of degree  $n - k$ :

$$g(x) = g_0 + g_1x + \dots + g_{n-k-1}x^{n-k-1} + x^{n-k}. \quad 3.6$$

Every codeword polynomial in the code can be expressed as a multiple of this generator:

$$c(x) = m(x)g(x). \quad 3.7$$

Since the degree of  $g(x)$  is  $n - k$  and the degree of  $c(x)$  is strictly less than  $n$  it follows that the degree of  $m(x)$  must be strictly less than  $k$  i.e:

$$m(x) = m_0 + m_1x + \dots + m_{k-1}x^{k-1}. \quad 3.8$$

This represents the encoding operation that maps  $k$  bits to  $n$  bits. There are  $k$  coefficients in  $m(x)$  justifying that the dimension of the code is  $k$  and there are  $n$  coefficients in  $c(x)$  justifying that the length of the code is  $n$ .

Every cyclic code is thus characterized by its generator polynomial, which is exactly why cyclic codes are much easier to describe and implement compared to arbitrary linear

codes: due to the cyclic structure of the code, encoding of the message polynomial

$$m(x) = m_0 + m_1x + \dots + m_{k-1}x^{k-1}, \quad \mathbf{3.9}$$

through Eq. 3.7 can be performed with a shift register, greatly reducing complexity and memory requirements. More specifically, the message sequence

$$[m_0 \ m_1 \ \dots \ m_{k-1} \ \underbrace{0 \ 0 \ \dots \ 0}_{n-k}]$$

is given as input (from left to right) into the shift register of Fig. 3.1. The shift register is initialized with zeros. Note that the shift register requires only  $n - k$  memory elements to encode the information sequence.

The reader should take a moment to verify that encoding through Eq. 3.7 and encoding with the shift register of Fig. 3.1 are indeed equivalent. In general, encoding cannot be made simpler and shift register encoding is one of the benefits cyclic codes enjoy compared to arbitrary linear block codes.

### Some useful definitions

The *Hamming weight* of a vector  $\mathbf{c}$ , denoted as  $w(\mathbf{c})$ , is the number of non-zero elements in the vector. The *Hamming distance* between two  $n$ -dimensional vectors  $\mathbf{c}_1$  and  $\mathbf{c}_2$ , denoted as  $d_H(\mathbf{c}_1, \mathbf{c}_2)$ , is the number of positions in which the two vectors differ:

$$d_H(\mathbf{c}_1, \mathbf{c}_2) = \sum_{i=1}^n [x_i \neq y_i]. \quad \mathbf{3.10}$$

For instance, the Hamming distance between vectors  $\mathbf{c}_1 = [1 \ 0 \ 1]$  and  $\mathbf{c}_2 = [1 \ 1 \ 0]$  is  $d_H(\mathbf{c}_1, \mathbf{c}_2) = 2$  and each vector has Hamming weight 2.

The *minimum weight* of a code  $\mathcal{C}$ , denoted as  $w_{min}$  is the smallest Hamming weight of any non-zero codeword, i.e:

$$w_{min} = \min_{\mathbf{c} \in \mathcal{C}, \mathbf{c} \neq \mathbf{0}} w(\mathbf{c}). \quad \mathbf{3.11}$$

The *minimum distance*  $d_{min}$  of a code  $\mathcal{C}$  is the smallest Hamming distance between any two codewords of the code.

For any linear code, the minimum distance satisfies  $d_{min} = w_{min}$ . To see this, note that for linear codes any linear combination of codewords is a codeword. An  $(n, k)$  code is often denoted as  $(n, k, d_{min})$  to specify the minimum distance.

### 3.2.1 The $\mathcal{G}(23, 12)$ Golay and $\mathcal{C}(31, 11)$ BCH Code

The Golay code, denoted as  $\mathcal{G}(23, 12)$ , is a rate 0.54 binary cyclic code with minimum distance  $d_{min} = 8$ . The BCH code, denoted as  $\mathcal{C}(31, 11)$  is a rate 0.35 binary cyclic code with minimum distance  $d_{min} = 11$ . The Golay code outputs 23 bits for every 12 bits arriving at the Golay encoder while the BCH code produces 31 coded bits for every 11 bits arriving at the BCH encoder.

Interestingly enough, the Golay code has been referred to as “the single most important error-correcting code” [17] and has generated much interest over the years. Similarly, BCH codes have attracted attention due to the fact that they can be constructed with specified minimum distances. Nevertheless, these codes have not supported the burden of applications their importance suggests: from a practical point of view, capacity approaching codes of long block length (such as LDPC codes [20]) are preferred. This situation is reversed in the context of bistatic backscatter where error correction codes of a) *short* codeword length and b) *low-complexity* encoding, appropriate for resource-constrained tags/sensors are strict design options.

Both the Golay  $\mathcal{G}(23, 12)$  and BCH  $\mathcal{C}(31, 11)$  code have unique monic codeword polynomial  $g_{\mathcal{G}}(x)$  and  $g_{\mathcal{C}}(x)$  of degree 11 and 20 respectively, that generate the codes. Such polynomials can be found in [17]:<sup>1</sup>

$$\begin{aligned} g_{\mathcal{G}}(x) &= 1 + x^2 + x^5 + x^6 + x^7 + x^9 + x^{11}, \\ g_{\mathcal{C}}(x) &= 1 + x^2 + x^4 + x^6 + x^7 + x^9 + x^{10} + x^{13} + x^{17} + x^{18} + x^{20}. \end{aligned} \tag{3.12}$$

---

<sup>1</sup> It takes considerable effort to prove both that the generator of Eq. 3.12 indeed corresponds to the Golay code as well as that the minimum distance of the resulting code is  $d_{min} = 8$ . Details are omitted here and can be found in [17].

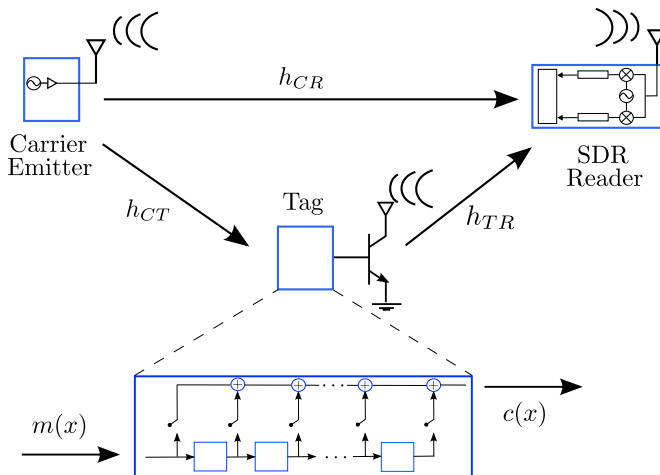


Figure 3.2: Encoding in ultra-low power, micro-controller unit (MCU)-based tags can be performed with a shift register encoder.

### 3.3 Encoding & ML Decoding for Block-coded Bistatic FSK

This section describes encoding at the tag and offers the optimum ML -also known as soft or unquantized- decision decoder for the coherent bistatic BFSK modulation scheme described in Chapter 2.

#### Encoding at the tags

The objective of encoding, performed directly by the RF tag, is to introduce the redundancy to the information to be reflected by mapping a sequence of  $k$  bits denoted as vector  $\mathbf{m} \in \{0, 1\}^k$  to  $n \geq k$  coded bits denoted as vector  $\mathbf{c} \in \{0, 1\}^n$ .

Utilizing the  $\mathcal{G}(23, 12)$  Golay code, the tag encodes  $k = 12$  information bits to produce  $n = 23$  coded bits while utilizing the BCH code  $n = 31$  coded bits are produced for every  $k = 11$  bits. Such encoding is performed at the tag using the low-complexity shift register encoder of Fig. 3.1 with the appropriate generator polynomial. Shift register encoding is ideal for ultra low-cost, low-power micro-controller based RF tags such as the ones utilized in this work. The coded bits can then be reflected in the same way as the uncoded bits (Fig. 3.2).

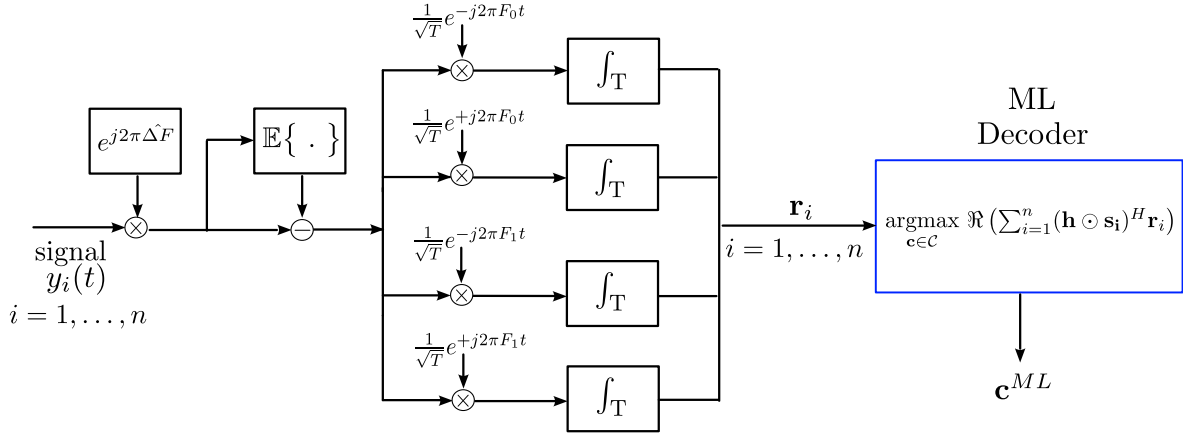


Figure 3.3: The structure of the coherent correlation decoder. The vector representations of  $n$  signals (one for each coded bit) are passed to the decoder. The decoder infers the transmitted codeword by selecting the most likely codeword (in the ML sense).

### ML Decoding for Coherent Bistatic FSK

The  $n$  coded bits are reflected by the tag and the receiver utilizes the processing chain given in Fig. 3.3. The noisy received signal for each coded bit is correlated with each of the 4 orthonormal basis functions and the resulting  $n$  vector representations are then passed to the decoder. The decoder exploits the information redundancy introduced by the tag by performing detection over a *sequence* of  $n$  bits belonging to the same codeword.

A maximum likelihood (ML) soft-decision decoder does this by maximizing the probability that a specific codeword was sent using the observed vector. To perform maximum likelihood decoding, all  $2^k$  possible vector codewords are listed at the receiver side and the probability of the received noisy vector, conditioned on each codeword, is evaluated. The codeword that maximizes the conditional probability is then selected as the estimate of the codeword sent. ML decoding is optimal (in the sense of minimizing the probability of decoding error) but has complexity exponential in the code dimension  $k$ ; for memory constrained RF tags, value  $k$  is necessarily small therefore the ML decoder is a practical option.

More specifically, let  $\mathcal{C}$  denote a cyclic block code and assume the tag encodes information sequence  $\mathbf{m}$  and subsequently reflects codeword

$$\mathbf{c} = [c_1 \ c_2 \ \dots \ c_n] \in \mathcal{C}. \quad \mathbf{3.13}$$

Assuming that the codeword length is strictly smaller than the channel coherence time, by Eq. 2.18 the SDR receives:

$$\mathbf{r}_i = \mathbf{h} \odot \mathbf{s}_i + \mathbf{n}_i, \quad i \in \{1, \dots, n\}, \quad 3.14$$

with  $\mathbf{s}_i = [1 - c_i \quad 1 - c_i \quad c_i \quad c_i]^T$ .

Then, assuming compound channel estimate  $\hat{\mathbf{h}}$  and equiprobable signaling, the optimal (in the sense of minimizing the probability of decoding error) decoding rule is given by:

$$\begin{aligned} \mathbf{c}^{ML} &= \operatorname{argmax}_{\mathbf{c} \in \mathcal{C}} p([\mathbf{r}_1 \quad \mathbf{r}_2 \quad \dots \quad \mathbf{r}_n] | \mathbf{c}, \hat{\mathbf{h}}) \\ &= \operatorname{argmax}_{\mathbf{c} \in \mathcal{C}} \prod_{i=1}^n p(\mathbf{r}_i | c_i, \hat{\mathbf{h}}) \\ &= \operatorname{argmax}_{\mathbf{c} \in \mathcal{C}} \prod_{i=1}^n \exp \left\{ -\frac{2}{N_0} \|\mathbf{r}_i - \hat{\mathbf{h}} \odot \mathbf{s}_i\|^2 \right\} \\ &= \operatorname{argmin}_{\mathbf{c} \in \mathcal{C}} \sum_{i=1}^n \|\mathbf{r}_i - \hat{\mathbf{h}} \odot \mathbf{s}_i\|^2 \\ &= \operatorname{argmin}_{\mathbf{c} \in \mathcal{C}} \sum_{i=1}^n -\Re \left( (\hat{\mathbf{h}} \odot \mathbf{s}_i)^H \mathbf{r}_i \right) \\ &= \operatorname{argmax}_{\mathbf{c} \in \mathcal{C}} \Re \left( \sum_{i=1}^n (\hat{\mathbf{h}} \odot \mathbf{s}_i)^H \mathbf{r}_i \right). \end{aligned} \quad 3.15$$

Note that for small block length cyclic codes such as the ones utilized in this work, the maximization of Eq. 3.15 can be performed with relatively low complexity.

### 3.4 Signal Diversity through Coding

Signal diversity is one of the most effective and widely employed techniques for improving the performance of wireless communication systems. It is based on the fact that in fading environments, the errors usually occur in bursts when the channel is in a deep fade; for bistatic scatter radio the probability of such deep fade is even larger due to the compound channel  $h_{CTR}$  which depends on the product of channel gains  $h_{CT}$  and  $h_{TR}$ . When the channel is in a deep fade, the code-bits of a specific codeword fade simultaneously and a (short block length) channel code is not powerful enough to correct the sheer amount of reception errors.

One method frequently employed is to use *time diversity*: the signal experiences independent fading by repeatedly transmitting it over multiple time slots whose separation is

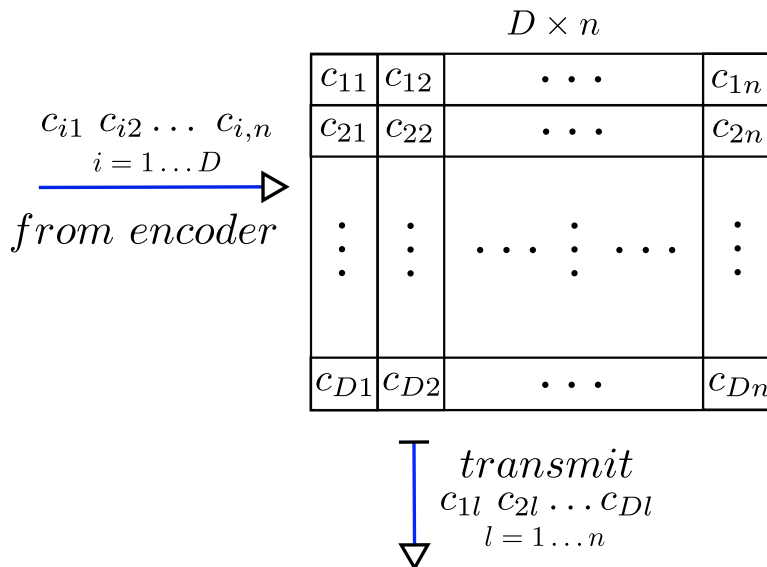


Figure 3.4: Matrix (block) interleaver: the tag stores a block of  $D$  codewords in a  $D \times n$  matrix and the information is transmitted column-wise. This way, fading affects bits of different codewords rather than consecutive bits of the same codeword.

greater than the channel coherence time  $T_{coh}$ . The receiver exploits the multiple instances of the received signal, each instant experiencing independent fading. Due to the repeated transmission of the same signal, time diversity can be viewed as a form of repetition coding provided that the bits has been *interleaved* prior to transmission. Repetition coding is however a trivial form of coding, motivating the use of more sophisticated channel codes, such as the cyclic codes considered in this work, for achieving signal diversity.

Signal diversity through channel coding is achieved through the matrix interleaving technique of Fig. 3.4, designed such that burst errors affect bits of different codewords rather than consecutive bits of the same codeword. The tag encodes and subsequently stores a block of  $D$  codewords in a  $D \times n$  matrix and the information is then transmitted column-wise. The receiver stores the  $Dn$  received symbols column-wise and performs ML decoding by Eq. 3.15 row-wise. This way, the receiver effectively decodes symbol sequences, which correspond to codewords with code-bits experiencing independent fading. The choice of the interleaver depth  $D$  depends on the channel coherence time. Specifically, for matrix interleaving as presented above, condition  $D \cdot T \geq T_{coh}$  must hold to guarantee that different code-bits experience independent fading.

The interleaving technique has the effect of considerably reducing the probability that

all code-bits with fade simultaneously. More specifically, it can be shown [19] (pp. 927) that as the depth of the interleaver  $D$  increases, ML decoding can achieve diversity of order  $d_{min}$ , where  $d_{min}$  denotes the minimum distance of the code. However, the interleaving technique introduces increased spacial and temporal overhead since the RF tag processes a block of  $D$  codewords upon transmission. Since the tag/sensor is equipped with limited memory, the interleaving technique as presented above may be a practical option only for relatively small values of  $D$ .

A more sophisticated method for achieving diversity is based on taking advantage of the mathematical structure of cyclic codes to minimize spacial and temporal requirements. If  $\mathcal{C}(n, k)$  is cyclic code with minimum distance  $d_{min}$  then interleaving  $\mathcal{C}$  to depth  $D$  produces a new code  $\mathcal{C}^D(Dn, Dk)$ . The new code is called an *interleaved* code, and it can be shown [17] (sec. 8.4) that the resulting code is cyclic and maintains a minimum distance of  $d_{min}$ . If  $g(x)$  is the generator of the original code, then  $g(x^D)$  generates the interleaved code. Therefore, the RF tag can readily generate the interleaved sequence with a shift register encoder of  $D(n - k)$  memory elements as opposed to processing  $D$  blocks of  $n$  bits, significantly reducing spacial and temporal overhead.

### 3.5 BER performance

Figs. 3.5–3.7 illustrate the bit error rate (BER) performance as a function of the average received SNR for the bistatic setup of Fig. 2.1. Each channel link is assumed i.i.d Rayleigh distributed, with  $\{h_{CR}, h_{CT}, h_{TR}\} \sim \mathcal{CN}(0, 1)$ . The tag modulates information at a rate of 1Kbps and the channel coherence time is assumed to span a limited number of 100 bits. During the channel coherence time,  $N_{tr} = 40$  training bits are utilized for estimating the channel characteristics with the LS approach of Eq. 2.35, and  $N = 60$  bits carry useful information. It is assumed that the receiver synchronizes without error and estimates the carrier frequency offset perfectly. Both the cyclic  $\mathcal{G}(23, 12)$  Golay code as well as the  $\mathcal{C}(31, 11)$  BCH code with generators by Eq. 3.12 are considered.

Regardless of the specific code utilized, any given codeword contains  $n - k$  redundant bits - which do not contain useful information- used to correct errors occurring during transmission. A transmission budget which allocates  $\mathcal{E}_b$  Joules/bit for the  $k$  bits of uncoded

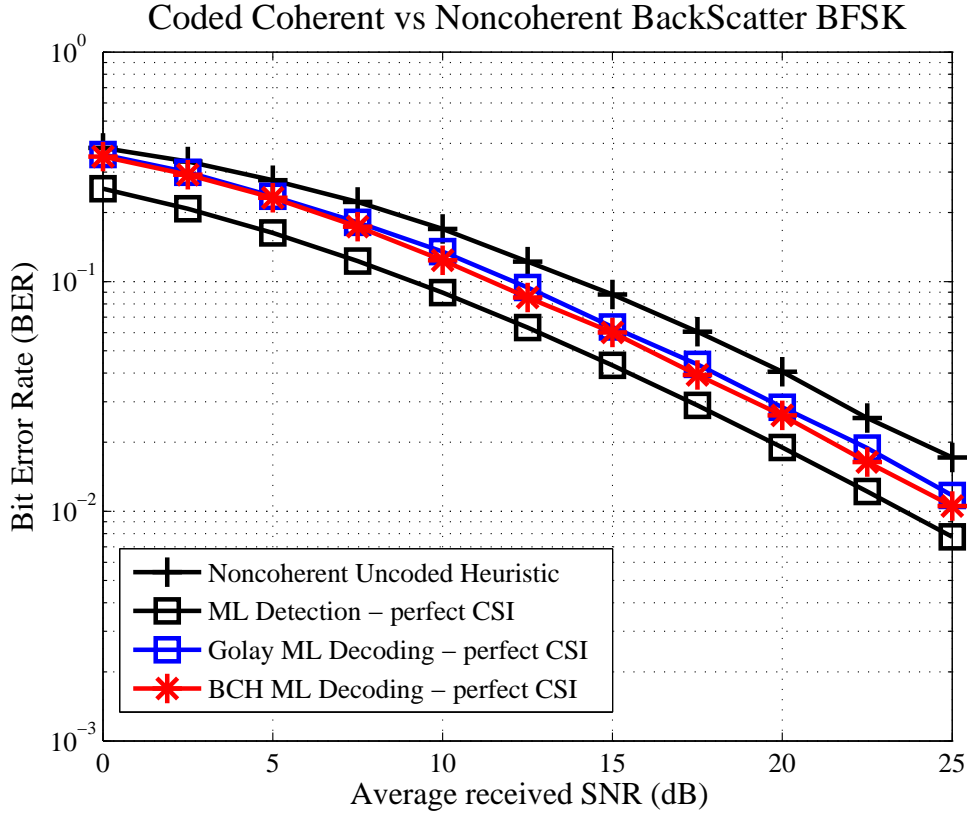


Figure 3.5: BER performance as a function of the average received SNR for uncoded noncoherent detection, uncoded coherent detection and coherent decoding with the Golay  $\mathcal{G}(23,12)$  and BCH  $\mathcal{C}(31,11)$  codes. A transmission budget is assumed, which spreads the available energy over the coded bits.

data must spread that energy over the  $n$  bits of coded data:

$$n\mathcal{E}'_b = k\mathcal{E}_b \implies \mathcal{E}'_b = \frac{k}{n}\mathcal{E}_b. \quad 3.16$$

Therefore, the transmission budget leads to a decrease in the energy allocated to each code-bit. Despite the energy reduction, the code must be able to correct the errors that manifest during transmission.

Fig. 3.5 depicts the bit error rate performance of coherent ML decoding with the  $\mathcal{G}(23,12)$  Golay and BCH  $\mathcal{C}(31,11)$  code assuming perfect channel estimation. Fig. 3.5 shows that both coding schemes degrade performance compared to coherent detection. Such results can be explained by the fact that the compound channel  $h_{CTR}$  increases the probability of a deep fading event; the limited error correction capability of the utilized

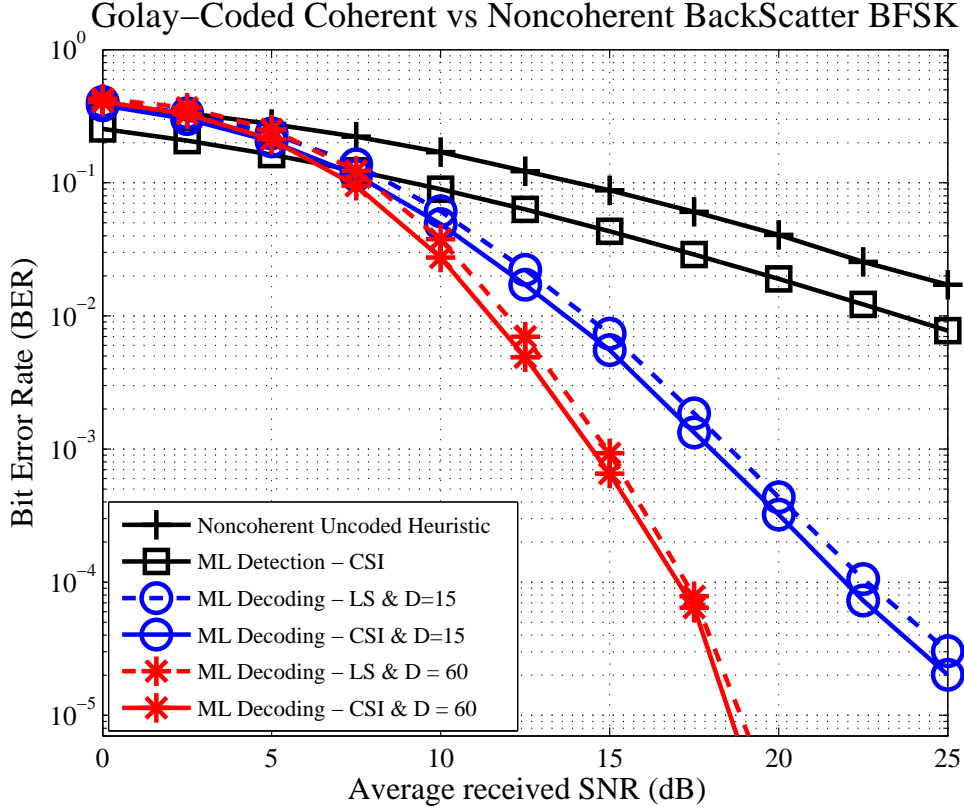


Figure 3.6: BER performance as a function of the average received SNR. Both uncoded noncoherent and coherent detection are considered as well as coherent decoding by Eq. 3.15 for the Golay  $\mathcal{G}(23, 12)$  code and various interleaving depths  $D$ .

codes cannot overcome the frequent deep-fading events. To bypass this issue, the interleaving technique of Sec. 3.4 is utilized.

Fig. 3.6 depicts the BER of interleaved coherent ML decoding with the  $\mathcal{G}(23, 12)$  Golay code assuming perfect channel estimation (labelled as CSI) and imperfect channel estimation with least squares (labelled as LS). It can be observed that increasing the interleaving depth  $D$  offers tremendous performance gains. Specifically, at  $\text{BER} = 10^{-2}$  the depth- ( $D = 15$ ) interleaved Golay code offers a coding gain of 10dB with perfect CSI and coding gain of 9.4dB with imperfect CSI compared to coherent detection. Similarly, comparing to coherent detection, the depth- ( $D = 60$ ) interleaved Golay code results in a 12,2dB coding gain with perfect CSI and coding gain of 11.7dB with imperfect CSI. Since the performance gap between the coherent and the noncoherent detector is approximately 4dB

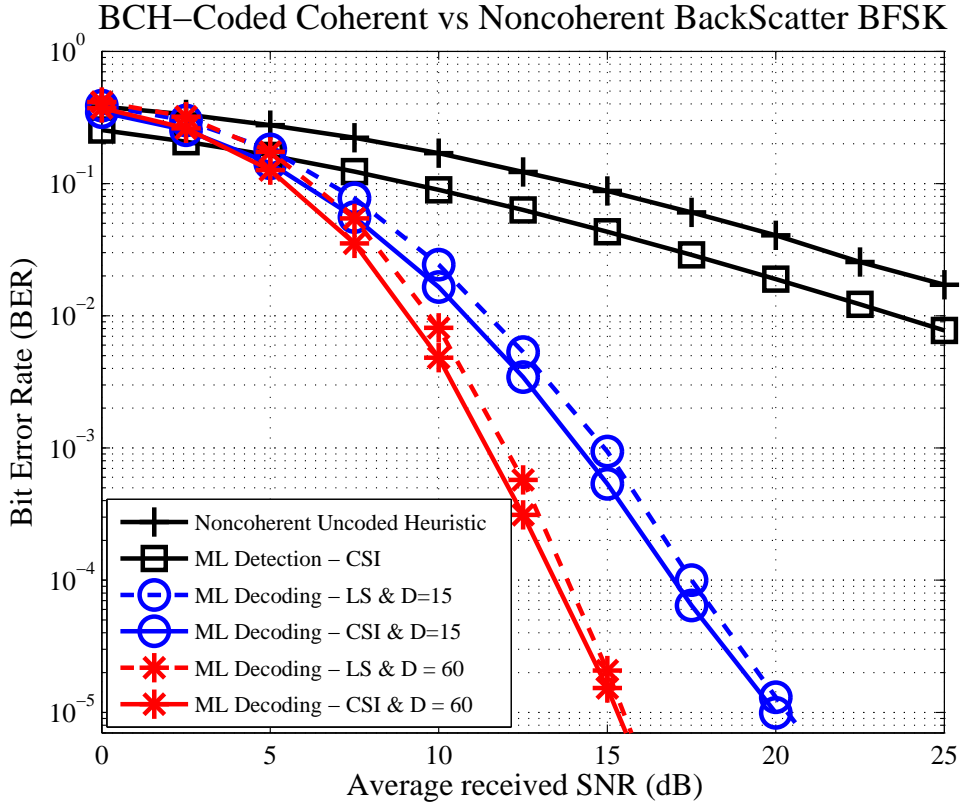


Figure 3.7: BER performance as a function of the average received SNR. Both uncoded noncoherent and coherent detection are considered as well as coherent decoding by Eq. 3.15 for the BCH  $\mathcal{C}(31, 11)$  code and various interleaving depths  $D$ .

at  $\text{BER} = 10^{-2}$ , the proposed coherent decoder outperforms the noncoherent detector by 16, 2dB assuming  $D = 60$  and perfect CSI.

Fig. 3.7 depicts the BER of interleaved coherent ML decoding utilizing the  $\mathcal{C}(31, 11)$  BCH code, again considering both perfect and imperfect channel estimation. It is observed that despite the rate reduction and hence the decrease in the energy per bit, the BCH code outperforms the Golay code with a performance gap of approximately 2.6 dB with  $D = 60$  at  $\text{BER} = 10^{-2}$ . Such result can be explained by the fact that (a) the minimum distance of the specific BCH code is  $d_{min}^{\mathcal{C}} = 11$  while the minimum distance of the Golay code is  $d_{min}^{\mathcal{G}} = 8$  and (b) since the BCH code produces longer coded sequences, for fixed channel coherence time the BCH code-bits are more likely to experience independent fading. Compared to the Golay code, the improved BER performance of the BCH code comes at the cost increased encoding complexity.



## Performance

### 4.1 Probability of Error for Coherent Bistatic FSK

#### 4.1.1 Conditional Probability of Error

Assuming equiprobable signaling and due to the symmetry of the constellation, it can be easily shown that:

$$p(e|\mathbf{h}) = p(e|h_{CTR}) = Q\left(\frac{\sqrt{T}|h_{CTR}|}{\sqrt{N_0}}\right). \quad 4.1$$

Substituting  $|h_{CTR}| = m_{CTR} = \sqrt{2P_c}|\Gamma_0 - \Gamma_1|a_{CT}a_{TR}\frac{2}{\pi}s$  by Eq. 2.8 of Sec. 2.1, the conditional probability of error can be expressed as a function of the average received signal-to-noise ratio,  $\overline{\text{SNR}}$ :

$$p(e|h_{CTR}) = p(e|a_{CT}, a_{TR}) = Q\left(\frac{a_{CT} a_{TR}}{\sigma_{CT} \sigma_{TR}}\sqrt{\overline{\text{SNR}}}\right). \quad 4.2$$

with the definition of the average SNR given by Eq. 2.15 in Sec. 2.1.

#### 4.1.2 Probability of Error

The probability of error is offered by averaging over  $h_{CTR}$  and is given by:

$$\begin{aligned} p(e) &= \mathbb{E}_{h_{CTR}} \{p(e|h_{CTR})\} \\ &= \mathbb{E}_{a_{CT}} \left\{ \mathbb{E}_{a_{TR}} \{p(e|a_{CT}, a_{TR})\} \right\} \\ &= \frac{1}{2} - \frac{\sqrt{\pi}}{4} \text{U}\left(\frac{1}{2}, 0, \frac{2}{\overline{\text{SNR}}}\right), \end{aligned} \quad 4.3$$

where  $U(a, b, z)$  denotes the *confluent hypergeometric*  $U$  function, given in integral form as:

$$U(a, b, z) = \frac{1}{\Gamma(a)} \int_{\mathbb{R}^+} e^{-zt} t^{a-1} (t+1)^{b-a-1} dt. \quad 4.4$$

More specifically:

$$\begin{aligned} p(e) &= \int_{\mathbb{R}} \int_{\mathbb{R}} Q\left(\frac{a_{CT} a_{TR}}{\sigma_{CT} \sigma_{TR}} \sqrt{\text{SNR}}\right) p(a_{TR}) p(a_{CT}) da_{TR} da_{CT} \\ &= \int_{\mathbb{R}} \int_{\mathbb{R}} Q\left(\frac{a_{CT}}{\sigma_{CT}} \sqrt{x \text{SNR}}\right) p(x) p(a_{CT}) dx da_{CT}, \end{aligned} \quad 4.5$$

where  $x \triangleq \frac{a_{TR}^2}{\sigma_{TR}^2} \sim \left| \mathcal{CN}(0, 1) \right|^2$ , i.e the square of a unit power Rayleigh random variable, is an exponential random variable with p.d.f:

$$p(x) = \begin{cases} e^{-x}, & x > 0 \\ 0, & \text{otherwise} \end{cases}. \quad 4.6$$

Substituting Eq. 4.6 in Eq. 4.5:

$$p(e) = \int_{\mathbb{R}} \underbrace{\int_{\mathbb{R}^+} Q\left(\frac{a_{CT}}{\sigma_{CT}} \sqrt{x \text{SNR}}\right) e^{-x} dx}_{=f(a_{CT})} p(a_{CT}) da_{CT}. \quad 4.7$$

The inner integral of Eq.4.7 can be computed as follows:

$$f(a_{CT}) = \int_{\mathbb{R}^+} Q\left(\sqrt{x \frac{a_{CT}^2}{\sigma_{CT}^2} \text{SNR}}\right) \frac{d}{dx} (-e^{-x}) dx.$$

Using integration by parts:<sup>1</sup>

$$f(a_{CT}) = \frac{1}{2} + \int_{\mathbb{R}^+} e^{-x} \frac{d}{dx} Q\left(\sqrt{x \frac{a_{CT}^2}{\sigma_{CT}^2} \text{SNR}}\right) dx. \quad 4.8$$

It can further be shown (proof is given in the Appendix) that:

$$\frac{d}{dx} Q\left(\sqrt{x \frac{a_{CT}^2}{\sigma_{CT}^2} \text{SNR}}\right) = -\sqrt{\frac{\frac{a_{CT}^2}{\sigma_{CT}^2} \text{SNR}}{8\pi}} \frac{1}{\sqrt{x}} e^{-\frac{1}{2} x \frac{a_{CT}^2}{\sigma_{CT}^2} \text{SNR}}. \quad 4.9$$

---

1

$$\int_a^b g(x) f'(x) dx = g(x) f(x) \Big|_a^b - \int_a^b g'(x) f(x) dx$$

Combining Eqs. 4.8-4.9 offers:

$$f(a_{CT}) = \frac{1}{2} - \sqrt{\frac{\frac{a_{CT}^2}{\sigma_{CT}^2} \overline{\text{SNR}}}{8\pi}} \int_{\mathbb{R}^+} \frac{1}{\sqrt{x}} e^{-x \left( \frac{1}{2} \frac{a_{CT}^2}{\sigma_{CT}^2} \overline{\text{SNR}} + 1 \right)} dx,$$

and using the relation  $\int_{\mathbb{R}^+} \frac{1}{\sqrt{x}} \exp\{-ax\} dx = \sqrt{\frac{\pi}{a}}$  yields

$$f(a_{CT}) = \frac{1}{2} - \frac{1}{2} \sqrt{\frac{\frac{a_{CT}^2}{\sigma_{CT}^2} \overline{\text{SNR}}}{\frac{a_{CT}^2}{\sigma_{CT}^2} \overline{\text{SNR}} + 2}}. \quad 4.10$$

Hence, by utilizing Eq. 4.10 and substituting in Eq. 4.7, the probability of error is given by:

$$p(e) = \frac{1}{2} - \frac{1}{2} \int_{\mathbb{R}} \sqrt{\frac{\frac{a_{CT}^2}{\sigma_{CT}^2} \overline{\text{SNR}}}{\frac{a_{CT}^2}{\sigma_{CT}^2} \overline{\text{SNR}} + 2}} p(a_{CT}) da_{CT}.$$

By substituting the p.d.f of  $a_{CT} \sim |\mathcal{CN}(0, \sigma_{CT}^2)|$ :

$$p(e) = \frac{1}{2} - \frac{1}{2} \int_{\mathbb{R}^+} \sqrt{\frac{\frac{a_{CT}^2}{\sigma_{CT}^2} \overline{\text{SNR}}}{\frac{a_{CT}^2}{\sigma_{CT}^2} \overline{\text{SNR}} + 2}} \frac{2a_{CT}}{\sigma_{CT}^2} e^{-\frac{a_{CT}^2}{\sigma_{CT}^2}} da_{CT}. \quad 4.11$$

Setting  $t = \frac{a_{CT}^2}{\sigma_{CT}^2} \overline{\text{SNR}}/2$ , the integral of Eq. 4.11 can be written as:

$$\begin{aligned} p(e) &= \frac{1}{2} - \frac{1}{2} \int_{\mathbb{R}^+} \sqrt{\frac{t}{t+1}} \frac{2}{\overline{\text{SNR}}} e^{-\frac{2}{\overline{\text{SNR}}}t} dt \\ &= \frac{1}{2} - \frac{1}{2} \underbrace{\int_{\mathbb{R}^+} \sqrt{\frac{t}{t+1}} \frac{d}{dt} \left( -e^{-\frac{2}{\overline{\text{SNR}}}t} \right) dt}_{=A}. \end{aligned} \quad 4.12$$

Using integration by parts, the integral of Eq. 4.12 can be simplified to:

$$\begin{aligned} A &= -\sqrt{\frac{t}{t+1}} \exp\left\{-\frac{2}{\overline{\text{SNR}}}t\right\} \Big|_0^{+\infty} + \int_{\mathbb{R}^+} \frac{d}{dt} \left( \sqrt{\frac{t}{t+1}} \right) \exp\left\{-\frac{2}{\overline{\text{SNR}}}t\right\} dt \\ &= 0 + \int_{\mathbb{R}^+} \frac{1}{2} t^{-\frac{1}{2}} (t+1)^{-\frac{3}{2}} \exp\left\{-\frac{2}{\overline{\text{SNR}}}t\right\} dt. \end{aligned} \quad 4.13$$

Substituting the above back in Eq. 4.12:

$$\begin{aligned} p(e) &= \frac{1}{2} - \frac{1}{2} \int_{\mathbb{R}^+} \frac{1}{2} t^{-\frac{1}{2}} (t+1)^{-\frac{3}{2}} \exp\left\{-\frac{2}{\overline{\text{SNR}}}t\right\} dt \\ &= \frac{1}{2} - \frac{\sqrt{\pi}}{4} \text{U}\left(\frac{1}{2}, 0, \frac{2}{\overline{\text{SNR}}}\right). \end{aligned} \quad 4.14$$

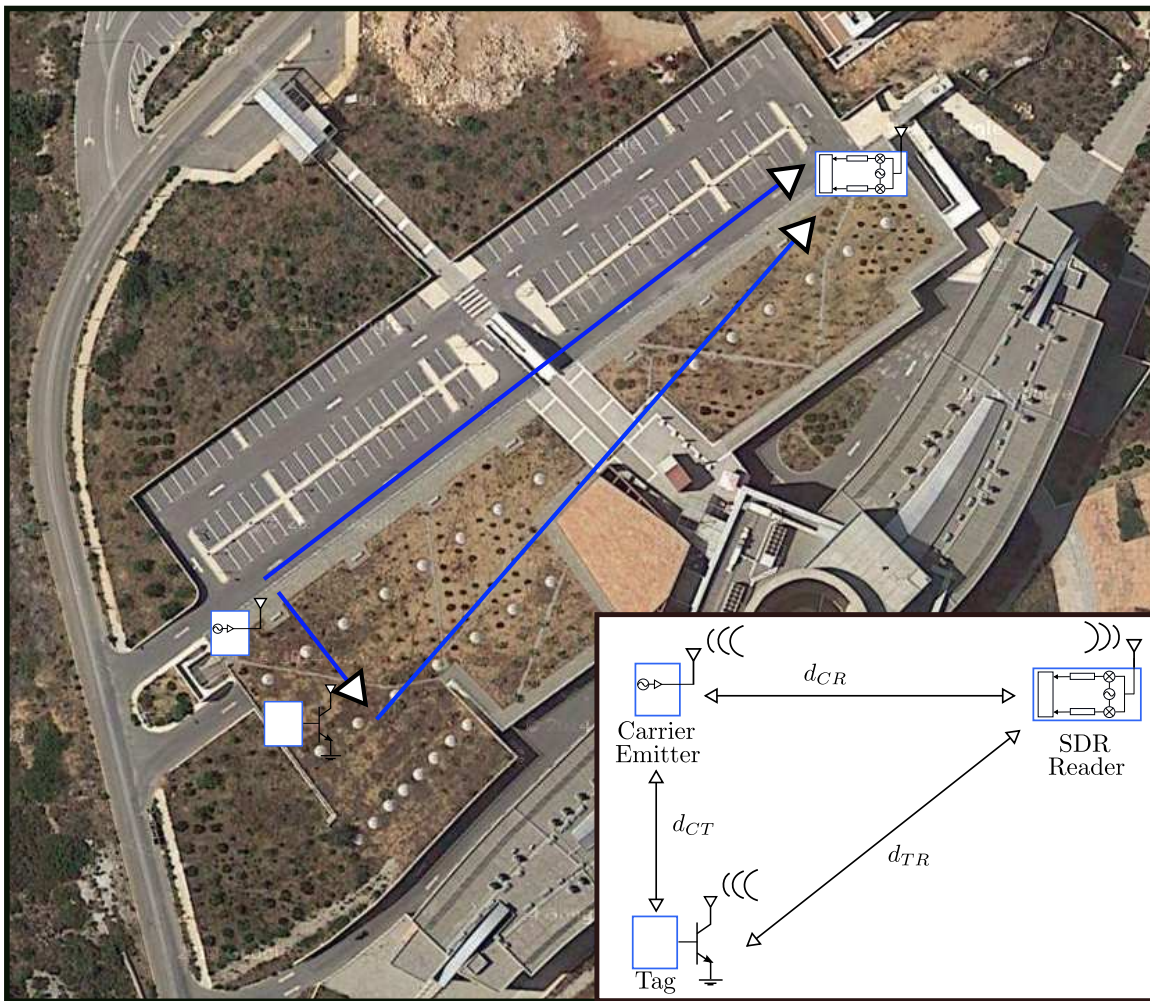


Figure 4.1: Bistatic experimental setup - The carrier emitter, RF tag and software-defined radio are placed on an open field. The distance between carrier emitter and RF tag is set to  $d_{CT} = 10\text{m}$ .

## 4.2 Experimental Results: Achieved Bistatic Ranges

Range measurements were conducted outdoors with the experimental setup of Fig. 4.4-left. A carrier emitter was set to transmit a carrier wave of frequency 868 MHz with 13dBm transmit power. A custom, programmable, semi-passive scatter radio tag with a monopole antenna was used to modulate at rate 1Kbps using the FSK modulation scheme presented in Chapter. 2. A USRP-2 software defined radio was utilized as the receiver, connected to a laptop running custom receiver scripts. Omnidirectional antennas were employed.

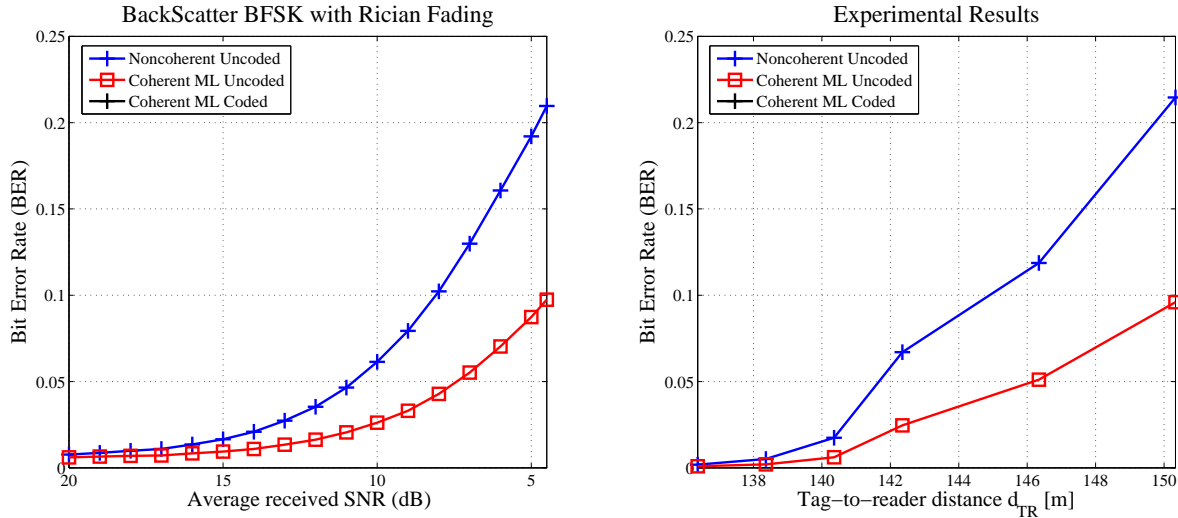


Figure 4.2: Right- Experimental bit error rate (BER) for noncoherent detection and ML coherent detection as a function of the tag-to-reader distance. Left- Simulated BER performance as a function of the average received SNR under Rician block-fading.

A packet of 30 training bits (known to receiver for synchronization) plus 31 bits corresponding to a BCH(31,11) codeword was utilized. Bit-wise detection by Eq. 2.26 was performed for the uncoded scenario while for the coded case the decoding rule of by Eq. 3.15 was employed. To maximize the achievable ranges, no energy budget was assumed and therefore the use of channel codes improves performance at the cost of rate reduction. In all considered scenarios CFO estimation was carried out with standard periodogram estimation techniques and synchronization was performed by correlating the received signal with the known training signal.

### 4.2.1 Scenario 1: Uncoded Bistatic Binary FSK

Fig. 4.2-right depicts the bit error rate as a function of the tag-to-reader distance for the aforementioned experimental setup utilizing both coherent and noncoherent receivers. It can be observed that with a carrier-to-tag distance of  $d_{CT} = 10\text{m}$  both coherent and noncoherent receivers achieve ranges on the order of 145m with  $\text{BER} \leq 10\%$ , corroborating the idea of bistatic scatter radio for increased-range sensing applications. It is noted that the reported BER on the order of 5% is acceptable for the considered low bit-rate sensing applications. More importantly, Fig. 4.2-right demonstrates that the offered coherent re-

ceiver produces range gains on the order of two-to-five meters compared to the noncoherent receiver under identical conditions, with negligible additional computational overhead (due to LS estimation).

It is also noted that in contrast to analysis of Chapter 2 the experimental performance gap between coherent and noncoherent detection changes dramatically with respect to the tag-reader distance (and hence receive SNR). Such result can be explained by the fact that the channel amplitudes  $a_{CT}$ ,  $a_{TR}$  and  $a_{CR}$  cannot be considered Rayleigh-distributed for the considered *open-field* obstacle-free scenario of Fig. 4.4. Due to the presence of strong line-of-sight (LOS) components, the channel attenuation parameters are in fact Ricean-distributed [25].

Fig. 4.2-left depicts the simulated performance of noncoherent and coherent detection when the channel attenuation parameters are distributed according to the Rice distribution, i.e with p.d.f:

$$p(a_l) = \begin{cases} 2(\kappa_l + 1)a_l e^{-(\kappa_l + 1)(a_l^2 + \frac{\kappa_l}{\kappa_l + 1})} I_0\left(2a_l\sqrt{\kappa_l(\kappa_l + 1)}\right), & a_l > 0 \\ 0, & \text{otherwise} \end{cases} \quad l \in \{CT, TR, CR\}, \quad 4.15$$

where  $I_0(\cdot)$  denotes the modified Bessel function of order zero.

The *Rice factor*  $\kappa$  expresses how many times stronger the LOS component is compared to the non-LOS component due to multipath. Such factors were given per channel link as  $\{\kappa_{TR} = 5, \kappa_{CT} = 20, \kappa_{CR} = 5\}$ . Comparison of Fig. 4.2-left and Fig. 4.2-right can be used to highlight the relative performance between detectors under Ricean fading and qualitatively describes the experimental results.

## 4.2.2 Scenario 2: Coded Bistatic Binary FSK

Fig. 4.3-right depicts the bit error rate as a function of the tag-to-reader distance for the experimental setup of Fig. 4.4, utilizing the BCH (31,11) code. The experimental results demonstrate that utilizing a short-block length low-complexity channel code increases ranges by eight-to-ten meters compared to the uncoded noncoherent case, albeit at the cost of rate reduction. Therefore, by employing short block length channel codes and simple decoding, scatter radio can provide increased coverage by serving larger geographical areas, further leveraging the adoption of backscatter sensor networks for ultra low-cost, ultra low-power environmental sensing applications.

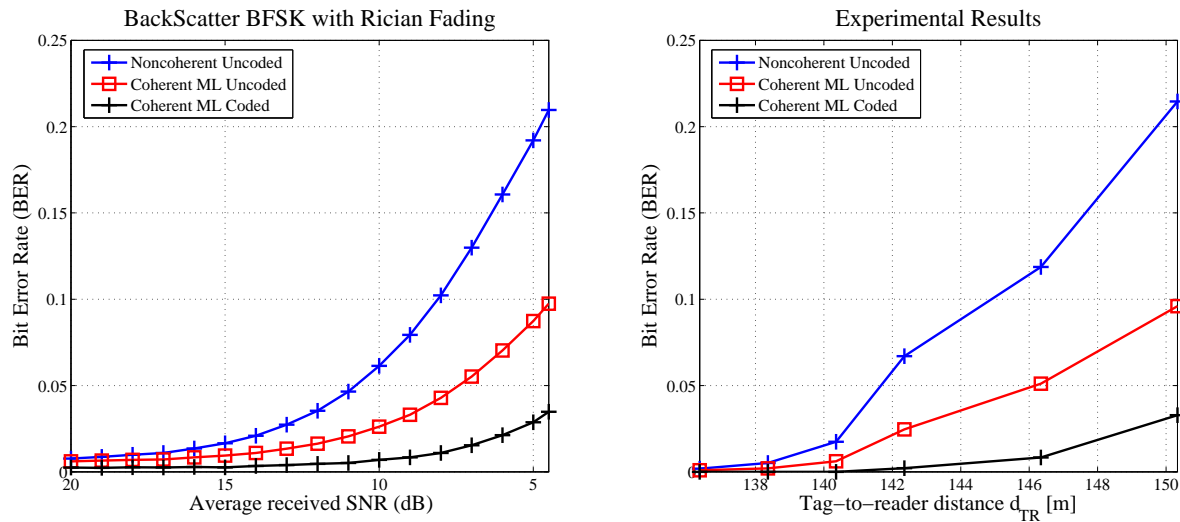


Figure 4.3: Right- Experimental bit error rate (BER) for noncoherent detection, ML coherent detection and ML decoding as a function of the tag-to-reader distance. Left- Simulated BER performance as a function of the average received SNR under Ricean block-fading.

The interleaving technique of Sec. 3.4 is not employed for the specific experimental case due to strong LOS components (or equiv. low probability of deep fading). Fig. 4.3-left depicts the simulated performance of the proposed channel code over the bistatic scatter radio channel with channel amplitudes distributed according to the Rice distribution and be used to qualitatively describe the experimental results by comparison with Fig. 4.3-right.

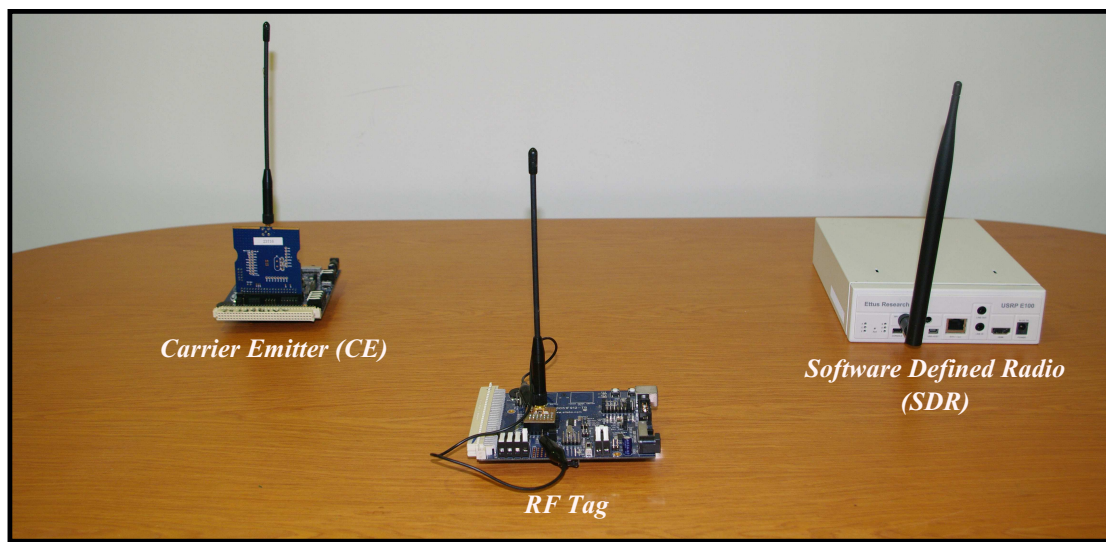


Figure 4.4: Custom carrier emitter, semi-passive scatter radio tag and a commodity SDR.



# Conclusions

## 5.1 Conclusions

This work proposed the first coherent reception algorithm for the bistatic scatter radio channel, expanding on recent work in [1]. Even though the bistatic setup in conjunction with scatter radio introduces multiple unknown channel and microwave/tag parameters, this work provided a simple solution for bit error rate reduction or equivalently range increase.

The optimal maximum likelihood coherent detector was derived and a simple procedure to estimate the channel characteristics was provided. Losses due to imperfect channel estimation were subsequently quantified by comparison with the analytical error performance of the system, which was also derived. Simulations revealed that the proposed detector offered significant performance gains compared prior art with or without assuming perfect channel estimate available at the receiver.

The performance of the system was further improved by proposing specific short-block length cyclic channel codes. The RF tag introduced redundancy to the reflected information (encoding) and the reader exploited such redundancy to improve BER performance (decoding). The proposed codes guaranteed minimum encoding complexity at the resource-constrained RF tag and optimum low-complexity maximum likelihood (ML) decoding at the reader. The structure of the specific codes was further exploited to perform low-complexity encoding in a way guaranteed to achieve high-order signal diversity. Performance gains of up to 18dB were demonstrated via simulations using the proposed channel codes.

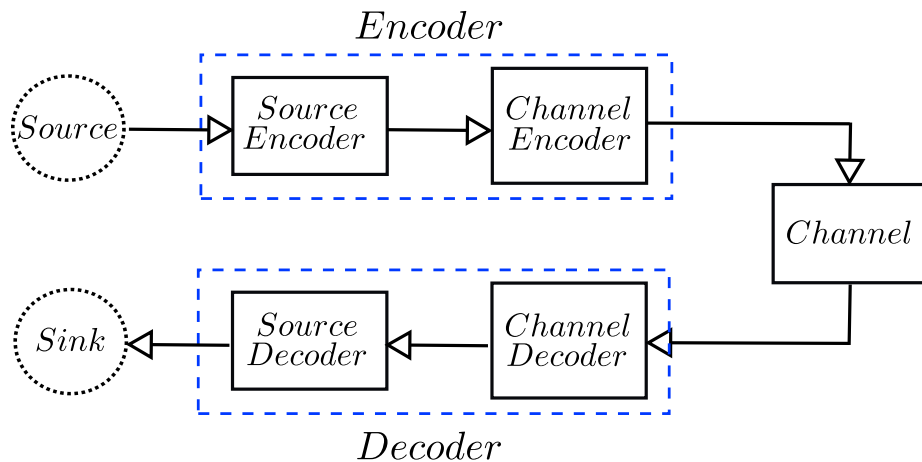


Figure 5.1: Challenge 1 - Exploiting joint source channel coding (JSCC) techniques to improve the system’s performance.

Experimental results were then conducted outdoors in an open field to characterize the effective range gains of the proposed detection/decoding schemes. A custom carrier emitter was set to transmit a sinusoid wave with as little as 20mW transmit power, illuminating a custom RF tag. A USRP-2 software defined radio acted as the receiver, connected to a laptop running custom receiver scripts. Using the specific setup, experimental ranges on the order of 100 meters were demonstrated and it was experimentally verified that the proposed detector offered range gains of 2 – 5 meters compared to prior art under identical conditions. The proposed decoder further increased range gains to 8 – 10 meters, compared to the uncoded setup.

Using the proposed receivers, scatter radio can provide increased coverage by serving larger geographical areas, further leveraging the adoption of backscatter sensor networks for ultra low-cost, ultra low-power environmental sensing applications.

## 5.2 Future Work

One interesting topic not addressed in this work is that of data compression at the tag, a process referred to as source coding. Interestingly enough, Shannon’s famous separation theorem states that there is no loss in optimality by performing source coding and channel coding separately and in a sequential manner. However this result holds only for asymptotically long block lengths and uncorrelated sources; neither condition holds for resource-

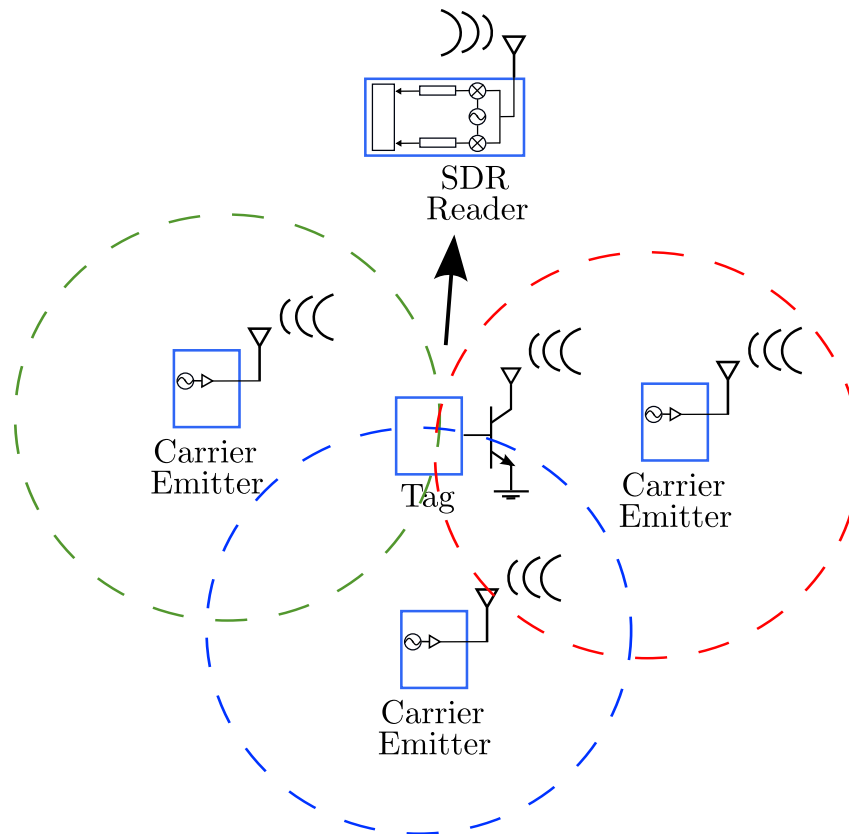


Figure 5.2: Challenge 2 - RSS-based tag localization with multiple emitters and signals measured directly at the reader.

contained tags measuring environmental conditions in a given area. Therefore, *joint source channel coding* techniques should be considered and potential performance benefits should be investigated (Fig. 5.1).

Large-scale backscatter sensor networks should be built, comprising of hundreds of low-cost low-power RF tags and limited number of carrier emitters. Such network will highlight practical design issues such as the placement of the tags relative to the emitters as well as the number of emitters. The emitters could be placed either stochastically or deterministically and could be either mobile -illuminating different subsets of tags at different time instances- or static. Emitters could perform FDMA or TDMA, or even perhaps a hybrid FDMA/TDMA scheme. What approach will be considered, what are the practical limits and what are the tradeoffs?

Large-scale dense networks, with hundreds of sensor tags, will require automated network self-localization: the measured quantities are meaningless without an indication of

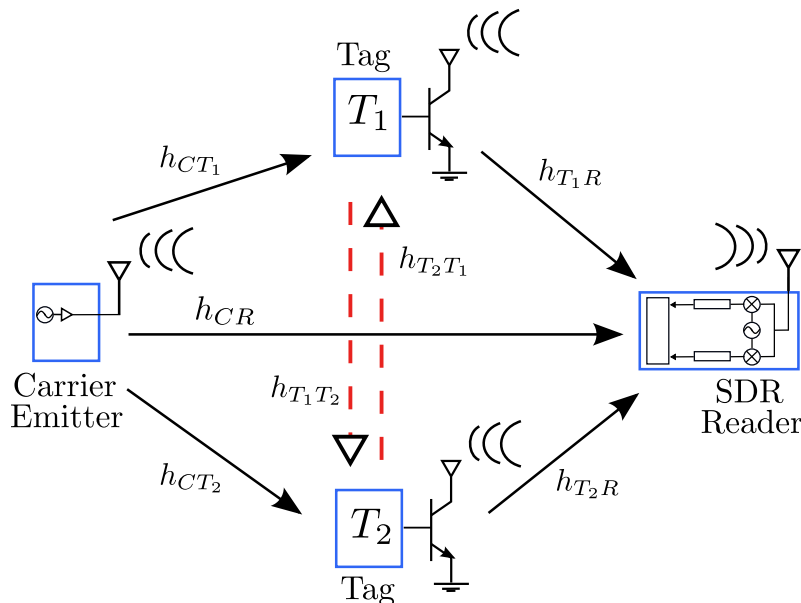


Figure 5.3: Challenge 3 - Designing a receiver to account for backscattered tag signals reflected by adjacent tags.

location. Could the emitters serve as known reference points used to infer the locations of the tags with received signal strength (RSS)-based techniques (Fig. 5.2)? If so, how many emitters should be placed in the immediate vicinity of an RF tag to accurately triangulate its location? Such questions will need to be carefully addressed (preliminary work and results can be found in [5]).

Another interesting question is what happens when two tags reflect signals while placed relatively close, as depicted in Fig. 5.3. Clearly, each tag will also reflect the reflected information from the other tag. A receiver could be designed to exploit this additional information, potentially offering performance gains.

The proposed receivers in conjunction with the proposed future directions offer tremendous potential for new wireless network sensor application, effectively overcoming limiting factors such as limited communication range, high monetary cost and high energy demands. With the imminent emergence of backscatter sensor networks as a key enabling technology, this work serves as a small step forward towards the realization of low-cost, low-power increased range sensing applications.

## Appendix

### 6.1 Independence of Projected Noise Components

Let  $\phi_1(t), \phi_2(t), \dots, \phi_k(t)$  denote  $k$  orthonormal basis functions of duration  $T$ , i.e:

$$\langle \phi_i(t), \phi_j(t) \rangle = \int_0^T \phi_i(t) \phi_j^*(t) dt = \begin{cases} 1, & i = j, \\ 0, & i \neq j, \end{cases}, \quad i, j = 1, \dots, k, \quad \mathbf{6.1}$$

assumed limited in the  $[-W, W]$  frequency band.

For complex baseband Gaussian random process  $n(t)$  with power spectral density  $\frac{N_0}{2}$  in the  $[-W, W]$  frequency band, the projection on an orthonormal basis  $\phi_i(t)$  is given by:

$$n_i = \langle n(t), \phi_i(t) \rangle = \int_0^T n(t) \phi_i^*(t) dt, \quad i = 1, \dots, k. \quad \mathbf{6.2}$$

Hence, noise components  $n_i$ ,  $i = 1, \dots, k$  are complex Gaussian random variables as linear combinations of the complex Gaussian random process  $n(t)$ . Then for  $i, j = 1, \dots, k$ :

$$\mathbb{E}\{n_i\} = \mathbb{E} \left\{ \int_{\mathbb{R}} n(t) \phi_i^*(t) dt \right\} = \int_{\mathbb{R}} \mathbb{E}\{n(t)\} \phi_i^*(t) dt = 0, \quad \mathbf{6.3}$$

and

$$\begin{aligned}
\mathbb{E}\{n_i n_j^*\} &= \mathbb{E}\left\{\int_{\mathbb{R}} n(t) \phi_i^*(t) dt \int_{\mathbb{R}} n^*(t) \phi_j(t) dt\right\} \\
&= \int_{\mathbb{R}} \int_{\mathbb{R}} R_n(s-t) \phi_i^*(s) \phi_j(t) ds dt \\
&= \int_{\mathbb{R}} \phi_j(t) \int_{\mathbb{R}} R_n(s-t) \phi_i^*(s) ds dt \\
&\stackrel{(a)}{=} \int_{\mathbb{R}} \phi_j(t) \int_{\mathbb{R}} e^{-j2\pi Ft} S_n(F) \Phi_i^*(F) dF dt \\
&\stackrel{(b)}{=} \frac{N_0}{2} \int_{\mathbb{R}} \phi_j(t) \int_{\mathbb{R}} e^{-j2\pi Ft} \Phi_i^*(F) dF dt \\
&\stackrel{(c)}{=} \frac{N_0}{2} \int_{\mathbb{R}} \phi_j(t) \int_{\mathbb{R}} \delta(s-t) \phi_i^*(s) ds dt \\
&\stackrel{(d)}{=} \frac{N_0}{2} \int_{\mathbb{R}} \phi_j(t) \phi_i^*(t) dt = \begin{cases} \frac{N_0}{2}, & i = j \\ 0, & \text{otherwise} \end{cases}.
\end{aligned} \tag{6.4}$$

where:

- $\{(a), (c)\}$  follow from Parseval's theorem,
- $(b)$  is due to the bandlimited basis function assumption,
- $(d)$  follows from the orthonormality assumption.

Hence, noise components  $n_i$ ,  $i = 1, \dots, k$  are complex Gaussian and are uncorrelated. Therefore, they are also independent:

$$\mathbf{n} = [n_1 \ n_2 \ \dots \ n_k] \sim \mathcal{CN}(0, \frac{N_0}{2} \mathbf{I}_k). \tag{6.5}$$

## 6.2 Derivative of $Q$ Function

This proof is based in whole on work in [15] and is given here translated from the original language for completeness of treatment.

By definition of the  $Q$  function:

$$\frac{d}{dx} Q\left(\sqrt{x \frac{a_{CT}^2}{\sigma_{CT}^2} \overline{\text{SNR}}}\right) = \frac{d}{dx} \left( \int_{\sqrt{x a_{CT}^2 \overline{\text{SNR}} / \sigma_{CT}^2}}^{+\infty} \frac{1}{\sqrt{2\pi}} \exp\left\{-\frac{\lambda^2}{2}\right\} d\lambda \right).$$

Let  $a(x) = \sqrt{x \frac{\sigma_T^2}{\sigma_C^2} \text{SNR}}$ ,  $g(\lambda) = \frac{1}{\sqrt{2\pi}} \exp\left\{-\frac{\lambda^2}{2}\right\}$  and

$$F(x) = \int_{a(x)}^{+\infty} g(\lambda) d\lambda.$$

The goal is then to compute:

$$\frac{d}{dx} F(x) \triangleq \lim_{\Delta x \rightarrow 0} \frac{F(x + \Delta x) - F(x)}{\Delta x}, \quad \mathbf{6.6}$$

where

$$\begin{aligned} \frac{F(x + \Delta x) - F(x)}{\Delta x} &= \frac{1}{\Delta x} \left( \int_{a(x+\Delta x)}^{+\infty} g(\lambda) d\lambda - \int_{a(x)}^{+\infty} g(\lambda) d\lambda \right) \\ &= \frac{1}{\Delta x} \left( \left[ \int_{a(x+\Delta x)}^{a(x)} g(\lambda) d\lambda + \int_{a(x)}^{+\infty} g(\lambda) d\lambda \right] - \int_{a(x)}^{+\infty} g(\lambda) d\lambda \right) \\ &= \frac{1}{\Delta x} \left( \int_{a(x+\Delta x)}^{a(x)} g(\lambda) d\lambda \right). \end{aligned} \quad \mathbf{6.7}$$

By utilizing the first order Taylor series expansion of function  $a(x)$ , Eq. **6.7** can be written as:

$$\begin{aligned} \frac{F(x + \Delta x) - F(x)}{\Delta x} &= \frac{1}{\Delta x} \left( \int_{a(x)+a'(x)\Delta x+O(\Delta x^2)}^{a(x)} g(\lambda) d\lambda \right) \\ &= \frac{1}{\Delta x} \left( \int_{a(x)+a'(x)\Delta x+O(\Delta x^2)}^{a(x)} G'(\lambda) d\lambda \right), \end{aligned}$$

where  $G'(\lambda) = \frac{d}{d\lambda} G(\lambda) = g(\lambda)$ .

Hence,

$$\begin{aligned} \frac{F(x + \Delta x) - F(x)}{\Delta x} &= \frac{1}{\Delta x} G(\lambda) \Big|_{a(x)+a'(x)\Delta x+O(\Delta x^2)}^{a(x)} \\ &= \frac{1}{\Delta x} \left( G(a(x)) - G(a(x) + a'(x)\Delta x + O(\Delta x^2)) \right) \\ &= \frac{1}{\Delta x} \left( G(a(x)) - G(a(x)) - G'(a(x))a'(x)\Delta x - O(\Delta x^2) \right), \end{aligned}$$

where in the last equality the first order Taylor series expansion of function  $G(a(x))$  has been utilized.

Substituting back in Eq. **6.6** and taking the limit yields:

$$\begin{aligned} \frac{d}{dx} F(x) &\triangleq \lim_{\Delta x \rightarrow 0} \frac{1}{\Delta x} \left( -G'(a(x))a'(x)\Delta x - O(\Delta x^2) \right) \\ &= -\lim_{\Delta x \rightarrow 0} \left( G'(a(x))a'(x) + O(\Delta x) \right) \\ &= -G'(a(x))a'(x) = \\ &= -g(a(x))a'(x). \end{aligned} \quad \mathbf{6.8}$$

Reinstating  $a(x) = \sqrt{x \frac{a_{CT}^2}{\sigma_{CT}^2} \overline{\text{SNR}}}$  and  $g(\lambda) = \frac{1}{\sqrt{2\pi}} \exp\left\{-\frac{\lambda^2}{2}\right\}$  into Eq. **6.8**:

$$\frac{d}{dx}F(x) = -\sqrt{\frac{\frac{a_{CT}^2}{\sigma_{CT}^2} \overline{\text{SNR}}}{8\pi}} \frac{1}{\sqrt{x}} \exp\left\{-\frac{1}{2}x \frac{a_{CT}^2}{\sigma_{CT}^2} \overline{\text{SNR}}\right\}, \quad \mathbf{6.9}$$

concluding the proof.

# Bibliography

- [1] J. Kimionis, A. Bletsas, and J. N. Sahalos, "Increased Range Bistatic Scatter Radio", *IEEE Trans. Commun.*, vol. 62, no. 3, pp. 1091-1104, Mar. 2014.
- [2] I. Akyildiz, W. Su, Y. Sankarasubramaniam, and E. Cayirci, "Wireless sensor networks: A survey," *Computer Networks*, vol. 38, no. 4, pp. 393-422, Mar. 2002.
- [3] P. N. Alevizos, N. Fasarakis-Hilliard, K. Tountas, N. Agadakos, N. Kargas, and A. Bletsas, "Channel Coding for Increased Range Bistatic Backscatter Radio: Experimental Results", in *Proc. IEEE RFID Technology and Applications (RFID-TA)*, Tampere, Finland, Nov. 2014, to appear.
- [4] P. N. Alevizos, "Channel coding and detection for increased range bistatic scatter radio", Master's thesis, Technical University of Crete, Nov. 2014, Supervisor A. Bletsas.
- [5] E. Alimpertis, "Smart sensors of RF and backscatter signals with localization", Master's thesis, Technical University of Crete, Aug. 2014, Supervisor A. Bletsas.
- [6] E. Arikan, "Channel polarization: A method for constructing capacity-achieving codes for symmetric binary-input memoryless channels", *IEEE Trans. Inf. Theory*, vol. 55, no.7, pp. 3051-3073, July 2009.
- [7] C. Berrou, A. Glavieux, and P. Thitimajshima, "Near Shannon limit error-correcting coding and decoding: Turbo codes", in *Proc. IEEE International Conference on Communications (ICC)*, Geneva, Switzerland, 1993, pp. 1064-1070.

- [8] A. Bletsas, A. G. Dimitriou, and J. N. Sahalos, "Improving backscatter radio tag efficiency", *IEEE Trans. Microw. Theory Tech.*, vol. 58, no. 6, pp. 1502-1509, Jun. 2010.
- [9] N. Fasarakis-Hilliard, P. N. Alevizos, and A. Bletsas, "Coherent detection and channel coding for bistatic backscatter communications", *Under preparation*.
- [10] E. Kampianakis, "Scatter Radio Sensor Network with Analog Frequency Modulation Principles", Master's thesis, Technical University of Crete, Jul. 2014, Supervisor A. Bletsas.
- [11] E. Kampianakis, J. Kimionis, K. Tountas, C. Konstantopoulos, E. Koutroulis, and A. Bletsas, "Wireless Environmental Sensor Networking with Analog Scatter Radio & Timer Principles", *IEEE Sensors J.*, Jun. 2014, *accepted*.
- [12] J. Kimionis, "Bistatic Scatter Radio for Increased-range Environmental Sensing", Master's thesis, Technical University of Crete, Aug. 2013, Supervisor A. Bletsas.
- [13] J. Kimionis, A. Bletsas, and J. N. Sahalos, "Design and Implementation of RFID Systems with Software Defined Radio", in *Proc. IEEE European Conf. on Antennas and Propagation (EuCAP)*, Prague, Czech Republic, Mar. 2012, pp. 3464-3468.
- [14] J. Kimionis, A. Bletsas, and J. N. Sahalos, "Bistatic backscatter radio for power-limited sensor networks", in *Proc. IEEE Global Commun. Conf. (Globecom)*, Atlanta, GA, USA, Dec. 2013, pp. 353-358.
- [15] A. P. Liavas, "Wireless Communication Systems (Course Notes)," School of ECE, Technical Univ. of Crete, Crete, 2013.
- [16] S. Lin, and D. J. Costello, "Error Control Coding", 2nd ed. Upper Saddle River, NJ: Prentice-Hall Inc., 2004.
- [17] R. J. McEliece, "The Theory of Information and Coding", 2nd ed. New York, NY: Cambridge University Press, 2001.
- [18] T. K. Moon, "Error Correction Coding, Mathematical Methods and Algorithms". Hoboken, NJ: Wiley-Interscience, 2005.

- [19] J. G. Proakis, and M. Salehi, "*Digital Communications*", 5th ed. New York, NY, 10020: McGraw-Hill, November 2007.
- [20] T. Richardson, and R. Urbanke, "*Modern Coding Theory*". New York, NY: Cambridge University Press, 2008.
- [21] A. P. Sample, D. J. Yeager, J. R. Smith, P. S. Powledge, and A. V. Mamishev, "Energy harvesting in RFID systems", in *Proc. International Conference on Actual Problems of Electron Devices Engineering (APEDE)*, Saratov, Russia, Sept. 2006, pp. 445-449.
- [22] A. Sample, J. Braun, A. Parks, and J. Smith, "Photovoltaic enhanced UHF RFID tag antennas for dual purpose energy harvesting", in *Proc. IEEE Intl. Conf. on RFID*, Orlando, Florida, Apr. 2011, pp. 146-153.
- [23] C. E. Shannon, "A mathematical theory of communication," *Bell System Technical Journal*, vol. 27, pp. 379-423, 1948.
- [24] H. Stockman, "Communication by means of reflected power", *Proc. IRE*, pp. 1196-1204, 1948.
- [25] D. Tse and P. Viswanath, "*Fundamentals of Wireless Communication*", New York, NY: Cambridge University Press, 2005.
- [26] S. Thomas, E. Wheeler, J. Teizer, and M. Reynolds, "Quadrature amplitude modulated backscatter in passive and semipassive UHF RFID systems" *IEEE Trans. Microw. Theory Tech.*, vol. 60, no. 4, pp. 1175-1182, Apr. 2012.
- [27] G. Vannucci, A. Bletsas, and D. Leigh, "A software-defined radio system for backscatter sensor networks", *IEEE Trans. Wireless Commun.*, vol. 7, no. 6, pp. 2170-2179, Jun. 2008.
- [28] D. J. Yeager, A. P. Sample, J. R. Smith, P. S. Powledge, and A. V. Mamishev, "Sensor applications in RFID technology", in *Proc. International Conference on Actual Problems of Electron Devices Engineering (APEDE)*, Saratov, Russia, Sept. 2006, pp. 449-452.